

# Relocating aftershocks of the 2017 Moiyabana, Botswana earthquake

Dagmar Ruth Bouwman

First supervisor: Hanneke Paulssen

Second supervisor: Matthew Herman

January 2019

## Abstract

During the temporary NARS-Botswana seismic network project, conducted by the Utrecht University to determine the structure of the crust and mantle beneath Botswana, a moment magnitude 6.5 earthquake occurred on April 3, 2017 in southeast Botswana near Moiyabana. The earthquake occurred inside the continental African plate, in an area with low historical seismic activity and more than 300 km away from the nearest seismically active fault structure, the Okavango Rift Zone. A sequence of 79 aftershocks followed the 2017 Moiyabana earthquake, with magnitudes between local magnitude 2.5 and body wave magnitude 5.0. In this study, the hypocenter locations and times of the main shock and the aftershocks are determined using the double-difference hypocenter location algorithm *hypoDD* [Waldhauser and Ellsworth (2000)]. The results of the relocation give more insight in the locations and geometries of the structures that slipped during the earthquake sequence and how they relate to the local geology. The relocated aftershocks form two clusters; the largest cluster contains the main event and 56 aftershocks and the smaller cluster contains 2 aftershocks, located 113 km away from the main event. The larger cluster of events is 24 km long in the NW-SE direction, consistent with the focal mechanism of the 2017 Moiyabana earthquake and local geological structures. The depth range of the events in the larger cluster is from  $0.107 \pm 0.611$  km to  $18.367 \pm 0.745$  km and the depth of the aftershocks decreases towards the northwest. The hypocenters are located on a northeast dipping fault. From these results I infer that the 2017 Moiyabana earthquake occurred on the reactivated Moiyabana fault, located in the Proterozoic Limpopo-Shashe belt. The Moiyabana Fault is part of an ancient zone of weakness, associated with the collision of the Kaapvaal and Zimbabwe Cratons, that responded to large scale extensional forces present in southern Africa.

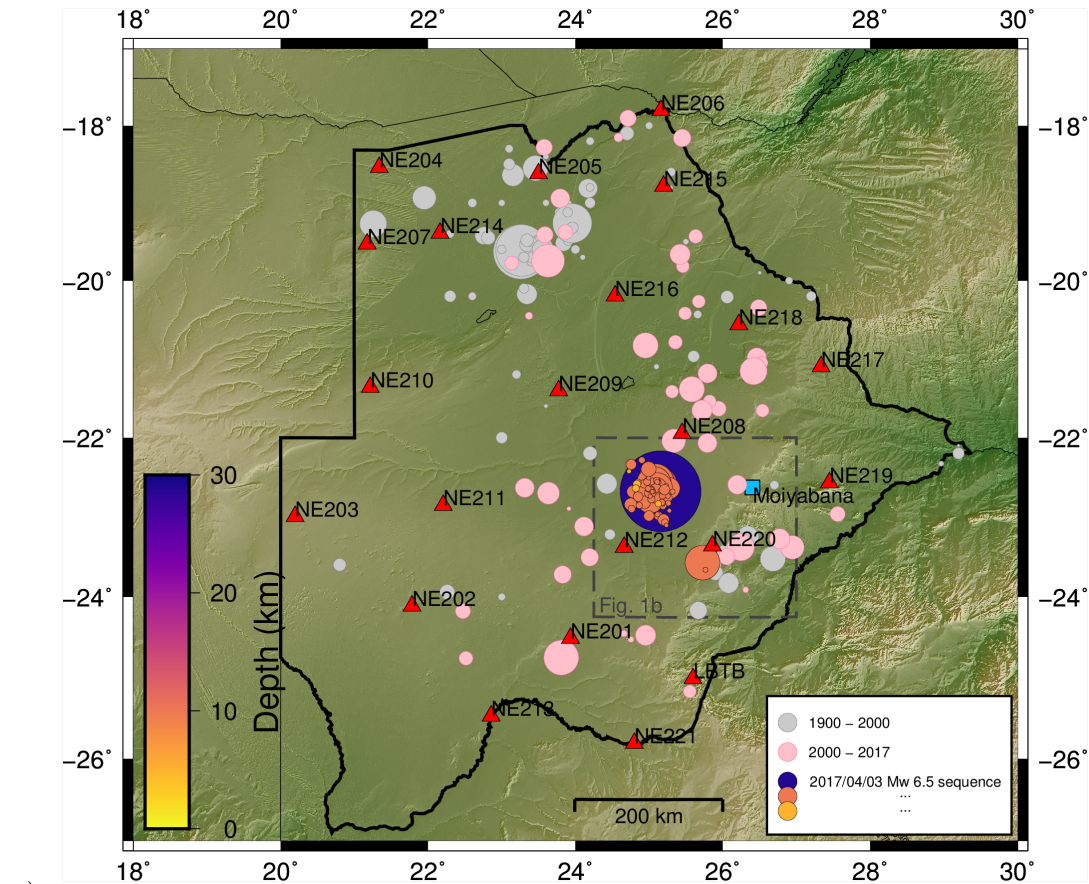
# 1 Introduction

On April 3, 2017 at 17:40:18.56 UTC a moment magnitude ( $M_w$ ) 6.5 earthquake occurred in the southeast of the Central District of Botswana, 132 km from the village Moiyabana (hereafter referred to as the Moiyabana earthquake). Whereas most of the global seismicity is associated with active faults near plate boundaries, this event happened inside the continental African plate. Large intraplate earthquakes are rare, but the occurrence of these events show that continental lithospheres are not entirely stable and are related to seismic hazards [England and Jackson (2011)]. The 2017 Moiyabana earthquake (with ID name: *2017/04/03Mw6.5*) occurred in an area with low historical seismic activity (Figure 1a) and there are not many strong earthquakes that have been recorded in the past. In the months following the main event, multiple aftershocks occurred that have to be relocated with respect to the main shock. The precise spatial offset between the hypocenters is needed to better constrain the geometries of the structures that slipped during the earthquakes.

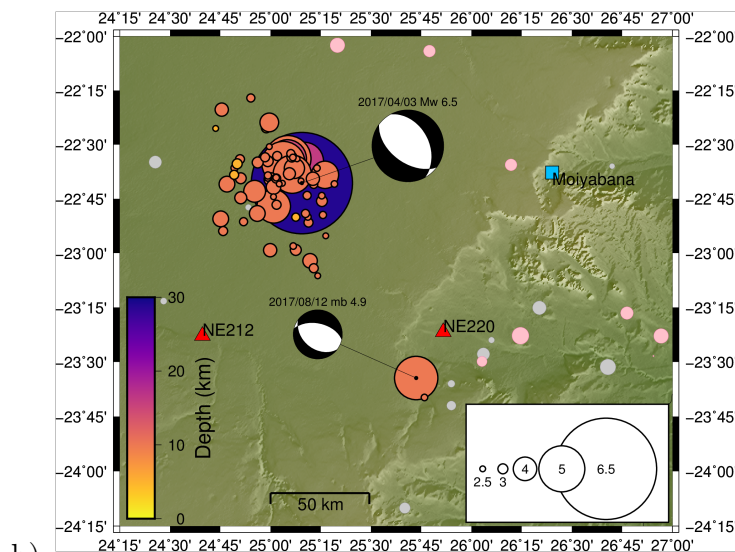
According to the [ISC On-line Bulletin \(2016\)](#), the hypocenter of the Moiyabana earthquake is at a depth of  $29 \pm 1.8$  km and located at  $22.678^\circ\text{S}$  and  $25.156^\circ\text{E}$  ( $\pm 7.5$  km). The focal mechanism of the event has a nodal plane with a strike of  $332^\circ$ , a dip of  $41^\circ$  and a rake of  $-70^\circ$ . A sequence of 79 aftershocks followed the 2017 Moiyabana earthquake, with magnitudes between local magnitude ( $M_L$ ) 2.5 and body wave magnitude ( $m_b$ ) 5.0. Two aftershocks have been recorded on August 12 2017, 113 km southeast from the main event. The last aftershock of the sequence was recorded at November 9 2017 [[ISC On-line Bulletin \(2016\)](#)]. The initial estimated locations of the main event and the aftershocks is given in Table A (Appendix A). The estimated locations, depths and magnitudes are shown in Figure 1, along with the LBTB and NARS-Botswana seismic stations and past seismic events.

The 2017 Moiyabana earthquake occurred within the Paleoproterozoic Limpopo-Shashe (LS) orogenic belt, which is situated between the Archean Kaapvaal and Zimbabwe Cratons, and event *2017/08/12mb4.9* occurred in the Kaapvaal Craton (Figure 2). The LS belt was formed during the collision between the Kaapvaal Craton and Zimbabwe Craton and is defined by crustal-scale thrust faults [Roering et al. (1992)]. Since the earthquakes occurred more than 300 kilometers away from the Okavango Rift Zone, a seismically active zone that has been suggested to belong to the southwestern part of the East African Rift Zone System (EARS) [Kinabo et al. (2007)], the events are classified as intraplate seismic events. Suggestions have been made that recent seismic activity in the LS belt point to the continuing southward propagation of the EARS [Bird et al. (2006); Materna et al. (2019)].

Using aeromagnetic and gravity data, Kolawole et al. (2017) found that the nodal plane of the Moiyabana earthquake aligns with a NW striking and NE dipping magnetic lineament within the Precambrian basement. This normal fault, named the Moiyabana Fault, had a displacement of 1.8 m and ruptured at 21-24 km depth [Kolawole et al. (2017)]. It has been suggested that the rupture occurred due to extensional reactivation of the Moiyabana Fault [Kolawole et al. (2017); Moorkamp et al. (2019)]. Figure 3 shows the interpreted geological structures by Kolawole et al. (2017).



a)



b)

**Figure 1:** a) Earthquake event location map for the 2017 Moiyabana earthquake and the aftershocks in Botswana. Every earthquake is represented by a colored circle. The pale colored circles are historical earthquakes. The darker colors inside the circles of the 2017 Moiyabana earthquake and its aftershocks indicate the depth of the hypocenters. The magnitude of every earthquake is given by the size of the circles. The event location, depth and magnitude information are from the [ISC On-line Bulletin \(2016\)](#) and the [USGS Earthquake Catalog \(2017\)](#). The light blue square gives the location of Moiyabana and the red triangles are the seismic stations from the LBTB and NARS-Botswana network. b) Zoomed map of the area inside the grey dashed box in Figure 1a). Focal mechanisms are from the *2017/04/03Mw6.5* and *2017/08/12mb4.9* events [H. Paulssen, personal communication].

Materna et al. (2019) found that both possible rupture planes, associated with the focal mechanism the main event, were able to fit the InSAR data within the level of the noise. However, a fault plane dipping towards the southwest was most favored from teleseismic waveform data and relocations done for three aftershocks [Materna et al. (2019)].

The aim of this study is to precisely relocate the aftershocks relative to the 2017 Moiyabana earthquake to better constrain the locations and geometries of the structures that slipped during the earthquake sequence and investigate how they relate to the local geology. The relocations are determined with the double-difference earthquake location algorithm *hypoDD* [Waldhauser and Ellsworth (2000)] using hand-picked P-wave arrival times from the LBTB and NARS-Botswana seismic networks. P-wave arrival times from other seismic networks within  $11^\circ$  of the main event are from the *ISC On-line Bulletin* (2016). I used three datasets for this study; one large dataset (A) and two smaller datasets (B and C). Datasets A and B contain initial estimated hypocenter locations and times of respectively 80 and 34 earthquakes, that are determined with a fixed depth below the surface ( $\geq 5$  km). Dataset C contains initial estimated hypocenter locations and times of 34 earthquakes that are determined with a fixed depth  $\geq 0$  km. Using different fixed depths gives different initial locations and times. Datasets B and C are used to find the right parameter settings for dataset A. In addition, the difference between using data from all seismic stations, including those outside Botswana (see Appendix E), and using only the data from the LBTB and NARS-Botswana seismic stations is investigated.

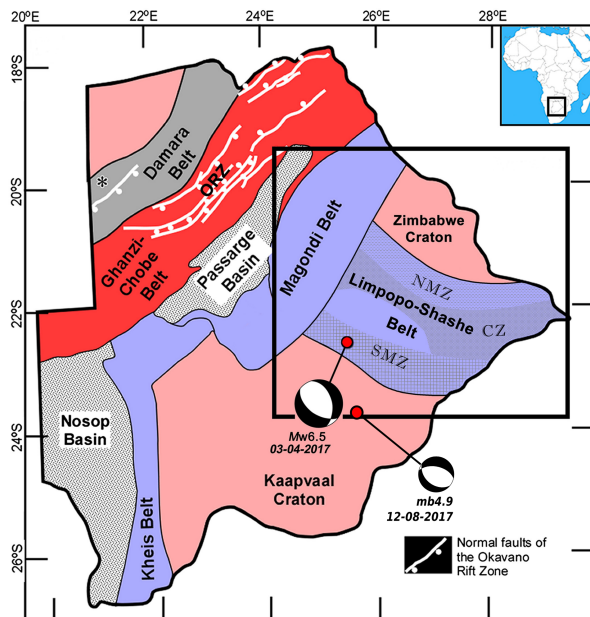


**Figure 2:** Modified Precambrian tectonic map of Botswana from Kolawole et al. (2017). The extent of the Archean Cratons, the Proterozoic belt and the epicenter and focal plane mechanism of the 2017 Moiyabana earthquake [USGS Earthquake Catalog (2017)] and the 2017/08/12mb4.9 aftershock [H. Paulssen, personal communication] are shown. The geological map is modified after Ranganai et al. (2002) and Leseane et al. (2015). The black box is not important for this study.

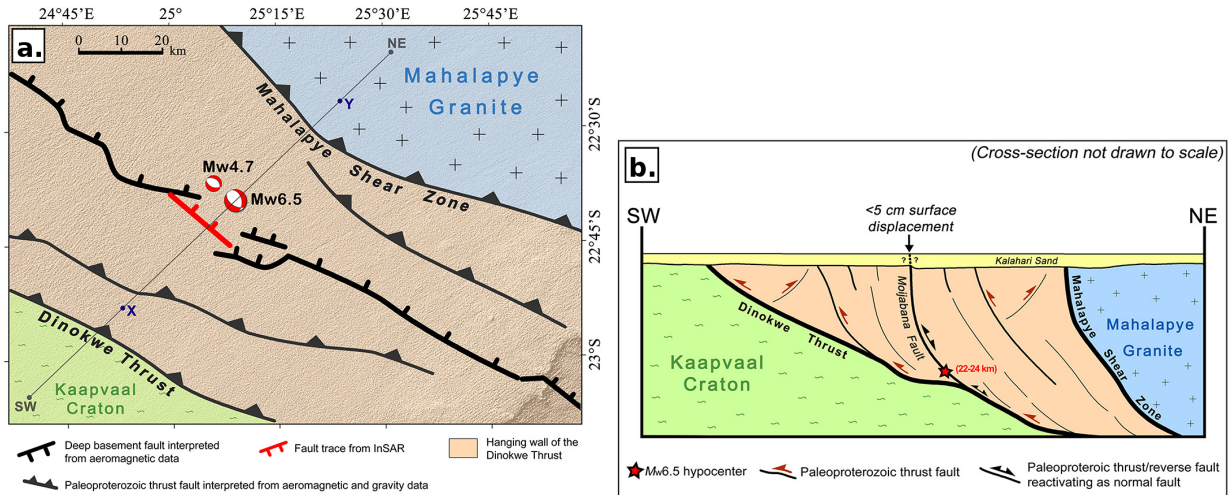


**Figure 3:** a) Interpretation of the tectonic setting of the 2017 Moiyabana earthquake and b) conceptual cross-section across Figure 3a by Kolawole et al. (2017), based on DInSAR, aeromagnetic and gravity data.

## 1.1 Geology

The hypocenter of the 2017 Moiyabana earthquake is in the southwestern part of the LS orogenic belt, between the Archean Zimbabwe Craton and Kaapvaal Craton (Figure 2), whereas the hypocenter of the *2017/08/12mb4.9* aftershock is in the Kaapvaal Craton. Based on structural and lithological characteristics, the Paleoproterozoic LS orogenic belt is divided into three zones: the Northern Marginal Zone (NMZ), the Central Zone (CZ) and the Southern Marginal Zone (SMZ) [Figure 2; McCourt and Vearncombe (1992); Ranganai et al. (2002)]. The epicenter of the Moiyabana earthquake is located in the SMZ. According to Ranganai et al. (2002), this part of the LS belt overlies the Kaapvaal Craton, in which the rocks are composed of tonalite-trondhjemite-granite assemblages and granulites. The crustal thickening in the LS belt, happening between  $\sim 2700$  and  $2650$  Ma ago, was a result of thrusting of the Kaapvaal Craton over the Zimbabwe Craton. The western part of the LS belt is truncated by the formation of the NE striking Magondi orogenic belt, which was caused by several post-Paleoproterozoic tectonic events. In the south of the LS belt, thrusting resulted in shortening in the direction of the southwest and in the NMZ it resulted in shortening in the direction to the north-northwest [Roering et al. (1992)]. During convergence, north-northeast dipping thrust faults appeared in the southern part of the LS belt and southwest dipping thrust faults in the northern part of the belt [Figure 4; Ranganai et al. (2002)]. Kolawole et al. (2017) interpreted multiple smaller scale northeast dipping thrust faults between the Dinokwe Thrust and the Mahalapye Shear Zone from DInSAR, aeromagnetic and gravity data (Figure 3a,b and Figure 1b). The 2017 Moiyabana earthquake epicenter is located within a crustal block of which the southwestern boundary is the Dinokwe Thrust and the northeastern boundary is the Mahalapye Shear Zone. There are no clear surface expressions from past deformations in this area, since it is covered with a 30 - 120 meters thick layer of Kalahari sand [Linol et al. (2013)].

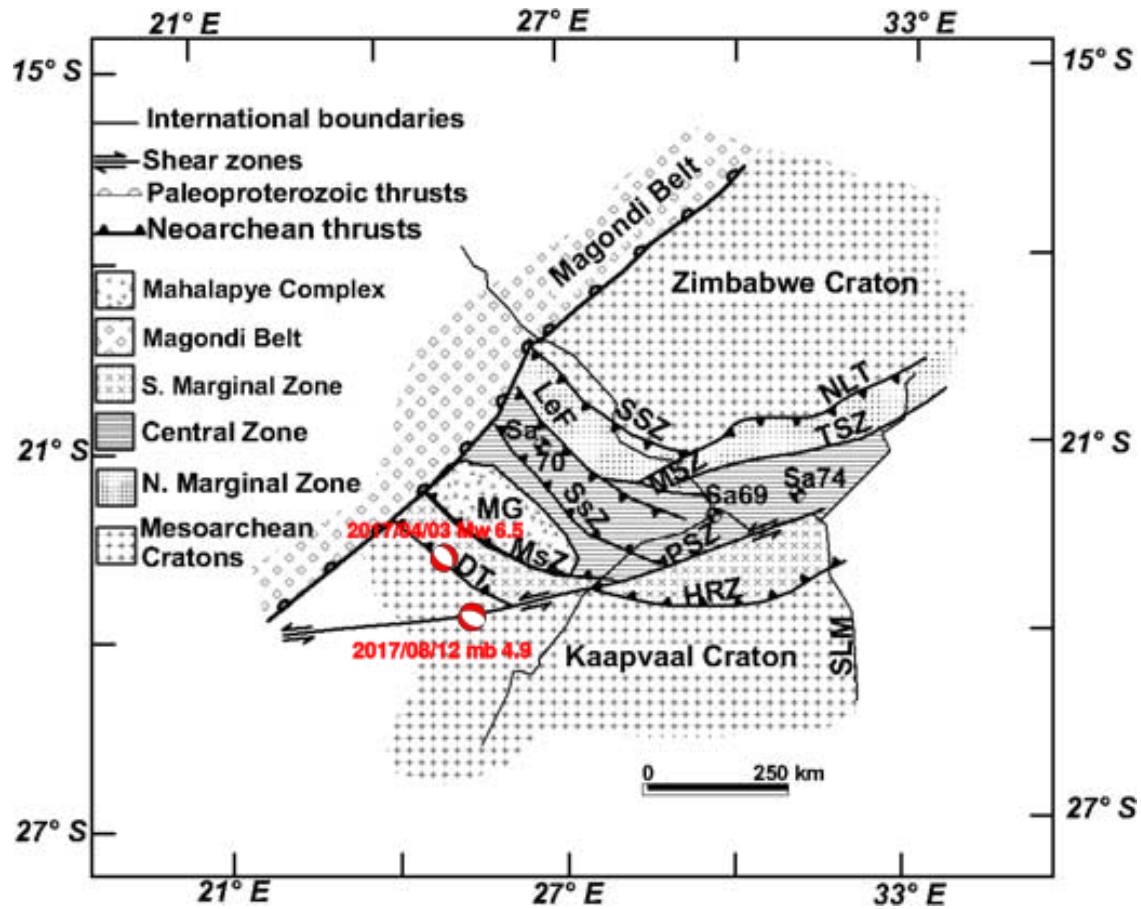


**Figure 4:** Modified map of the tectonic zones and fault structures of the Limpopo-Shashe Belt, Zimbabwe Craton and Kaapvaal Craton and Magondi belt, interpreted from gravity data and surface geology by [Ranganai et al. \(2002\)](#). The locations and focal mechanisms of events *2017/04/03 Mw 6.5* and *2017/08/12 mb 4.9* [H. Paulssen, personal communication] are shown in red. DT = Dinokwe Thrust; HRZ = Hout River Shear Zone; LeF = Lechana Fault; MG = Mahalapye Granite; MSZ = Magogaphate Shear Zone; MsZ = Mahalapye Shear Zone; NLT = Northern Limpopo Thrust Zone; PSZ = Palala Shear Zone; SLM = Sabi-Lebombo Monocline; SSZ = Shashe Shear Zone; SsZ = Sunny Side Shear Zone.

## 2 Methods

The determination of absolute hypocenter locations, for example done by the USGS or ISC, can have large uncertainties. The accuracy of the determination is controlled by factors such as: network geometry, available phases, the accuracy in arrival-time reading and knowledge of the Earth structure [Pavlis (1986); Gomberg et al. (1990)]. The effects that come from the errors in the Earth structure, represented as a seismic velocity model, can be reduced by using relative earthquake location methods [Poupinet et al. (1984); Frechet (1985); Got et al. (1994); Frémont and Malone (1987)].

To determine the relative locations of the 2017 Moiyabana aftershocks, I used the double-difference earthquake location algorithm implemented in *hypoDD* [Waldhauser and Ellsworth (2000)]. This section will discuss the *hypoDD* algorithm and the *hypoDD* relocation procedure, along with the types of data that have been used for this research.

### 2.1 HypoDD

The program *hypoDD* is designed to determine relative hypocenter locations of small and large numbers of earthquakes. The program, developed by Waldhauser and Ellsworth (2000), uses the differential travel time residuals between pairs of events. The difference in travel times (differential travel times) between pairs of events are determined from P- and S-wave travel time picks and/or cross-correlation measurements. The differential travel time residuals, also called double-difference residuals, are the differences between the predicted differential travel times and the observed differential travel times.

*HypoDD* works on the principle that the ray paths of two earthquakes going to the same station are similar along most of the entire ray path if the hypocentral distance between the two events is small compared to both the event-station distance and the scale length of velocity structure heterogeneity [Frechet (1985); Got et al. (1994)]. If pairs of events meet these conditions, then the difference in travel times between the two events, observed at a common station, can be attributed to the spatial offset between the two events. Except when the ray paths in a small region have a different source, then the absolute errors are not of a common origin [Waldhauser and Ellsworth (2000)].

In *hypoDD* the double-difference residuals for pairs of earthquake events at each station are minimized while linking together all observed event-station pairs. This is done by weighting the least squares with the singular value decomposition (SVD) method or the conjugate gradients method (LSQRS) [Paige and Saunders (1982)]. A least-squares solution for the inversion is found by adjusting the vector difference between hypocentral pairs during each iteration. After each iteration, the locations and partial derivatives are updated. Since the double-difference equations are linearized, corrections for the stations are needless [Waldhauser and Ellsworth (2000); Waldhauser (2001)].

### 2.1.1 Algorithm

The following explanation of the *hypoDD* algorithm is based on the paper by [Waldhauser and Ellsworth \(2000\)](#). First, the arrival time of a wave is calculated by adding the origin time of an earthquake and the travel time of the wave.

$$T_k^i = \tau^i + \int_i^k u ds \quad (1)$$

Equation (1) describes the arrival time  $T_k^i$  for earthquake event  $i$  at station  $k$ . The origin time of event  $i$  is given by  $\tau^i$ . Ray theory is used to calculate the travel time from event  $i$  to station  $k$ . To do so, a path integral from  $i$  to  $k$  of the slowness field  $u$  is taken, where the slowness field is the reciprocal of the velocity field.

The arrival time depends on the event parameters  $\mathbf{m}^i = (x^i, y^i, z^i, \tau^i)$  of event  $i$  and the station parameters  $(x_k, y_k, z_k)$  and  $T_k^i$  is not a linear function of  $(x^i, y^i, z^i)$ . In order to get a linearized Equation (1), a first order Taylor series expansion is applied to our problem. For  $f(x)$  it is given by

$$f(x) = f(x_0) + \left. \frac{df}{dx} \right|_{x=x_0} \Delta x \quad (2)$$

Rewriting Equation (2) gives

$$f(x) - f(x_0) = \left. \frac{df}{dx} \right|_{x=x_0} \Delta x. \quad (3)$$

In Equation (3),  $f(x)$  at position  $x$  is the measured (or observed) function,  $f(x_0)$  is the predicted (or calculated) function at  $x_0$  and  $\Delta x = (x - x_0)$ . The residual,  $r_k^i$ , of the arrival time is the difference between the observed arrival time and the calculated arrival time

$$r_k^i = (T^{obs} - T^{cal})_k^i \quad (4)$$

Since the origin time cancels, the residual is the same as the difference in the observed and calculated travel time ( $t_k^i$ ). This yields the travel time residual

$$r_k^i = (t^{obs} - t^{cal})_k^i. \quad (5)$$

Applying the first order Taylor expansion to the travel time residual gives

$$\begin{aligned}
r_k^i &= (t^{obs} - t^{cal})_k^i \\
&= \frac{\partial t_k^i}{\partial x}(x^i - x_0^i) + \frac{\partial t_k^i}{\partial y}(y^i - y_0^i) + \frac{\partial t_k^i}{\partial z}(z^i - z_0^i) + \frac{\partial t_k^i}{\partial \tau}(\tau^i - \tau_0^i) \\
&= \frac{\partial t_k^i}{\partial x}\Delta x^i + \frac{\partial t_k^i}{\partial y}\Delta y^i + \frac{\partial t_k^i}{\partial z}\Delta z^i + \frac{\partial t_k^i}{\partial \tau}\Delta \tau^i = \frac{\partial t_k^i}{\partial x}\Delta x^i + \frac{\partial t_k^i}{\partial y}\Delta y^i + \frac{\partial t_k^i}{\partial z}\Delta z^i + \Delta \tau^i \\
&= \frac{\partial t_k^i}{\partial \mathbf{m}}\Delta \mathbf{m}^i.
\end{aligned} \tag{6}$$

In this equation  $\Delta \mathbf{m}^i = (\Delta x^i, \Delta y^i, \Delta z^i, \Delta \tau^i)$ , the differences between the observed and calculated event parameters. Equation (6) can be used in the case of measured arrival times. This cannot be done when cross-correlation methods are used, because in that case travel time differences are measured between two events  $i$  and  $j$ . The travel time difference is then expressed as  $(t_k^i - t_k^j)^{obs}$ .

An equation for the relative hypocenter parameters between two events  $i$  and  $j$  is obtained by [Frechet \(1985\)](#). He did this by taking the difference of equation (6) for pair of events.

$$dr_k^{ij} = \frac{\partial t_k^{ij}}{\partial \mathbf{m}}\Delta \mathbf{m}^{ij} \tag{7}$$

The change in the relative hypocenter parameters between two events is given by  $\Delta \mathbf{m}^{ij} = (\Delta dx^{ij}, \Delta dy^{ij}, \Delta dz^{ij}, \Delta d\tau^{ij})$ . The partial derivatives in Equation (7) are the components of the slowness vector of the ray that connects the source and receiver, measured at the source. Considering the assumption of a similar slowness vector for the event pairs, the source is represented as the centroid between the two events. The assumption of a similar slowness vector is only valid for events that are close enough together.

The residual (from Equation (7)) between the observed and calculated differential travel time between the two events (Equation (8)), is called the double-difference:

$$dr_k^{ij} = (t_k^i - t_k^j)^{obs} - (t_k^i - t_k^j)^{cal} \tag{8}$$

An equation that gives the change in hypocentral distance between two events  $i$  and  $j$  is acquired by using Equation (6) and taking the difference between the two events. For this case, the appropriate slowness vector and origin time for each event are used.

$$\begin{aligned}
dr_k^{ij} &= \frac{\partial t_k^i}{\partial x}(x^i - x_0^i) + \frac{\partial t_k^i}{\partial y}(y^i - y_0^i) + \frac{\partial t_k^i}{\partial z}(z^i - z_0^i) + (\tau^i - \tau_0^i) \\
&\quad - \frac{\partial t_k^j}{\partial x}(x^j - x_0^j) - \frac{\partial t_k^j}{\partial y}(y^j - y_0^j) - \frac{\partial t_k^j}{\partial z}(z^j - z_0^j) - (\tau^j - \tau_0^j), \\
&= \frac{\partial t_k^i}{\partial x} \Delta x^i + \frac{\partial t_k^i}{\partial y} \Delta y^i + \frac{\partial t_k^i}{\partial z} \Delta z^i + \Delta \tau^i \\
&\quad - \frac{\partial t_k^j}{\partial x} \Delta x^j - \frac{\partial t_k^j}{\partial y} \Delta y^j - \frac{\partial t_k^j}{\partial z} \Delta z^j - \Delta \tau^j \\
&= \frac{\partial t_k^i}{\partial \mathbf{m}} \Delta \mathbf{m}^i - \frac{\partial t_k^j}{\partial \mathbf{m}} \Delta \mathbf{m}^j
\end{aligned} \tag{9}$$

The partial derivatives of the travel times are calculated for the first estimate of the original hypocenters and the location of the station where the arrival time is measured. The changes in hypocenter parameters, that are needed to fit the data, are given by  $\Delta x$ ,  $\Delta y$ ,  $\Delta z$  and  $\Delta \tau$ . An example of two relocation vectors ( $\Delta x_i$  and  $\Delta x_j$ ), that best fit the data and obtained from Equation (9), is shown in Figure 5. This figure (Figure 5) illustrates the double-difference earthquake relocation algorithm.

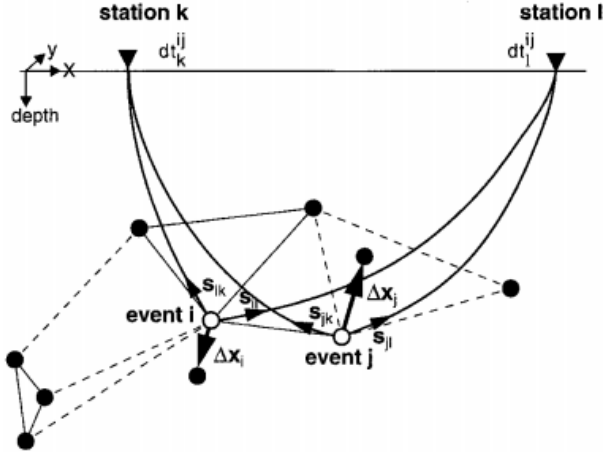


**Figure 5:** Overview of the the double-difference earthquake relocation algorithm from the paper by [Waldhauser and Ellsworth \(2000\)](#). The initial locations of event  $i$  and  $j$  are given by open circles. These events are linked to other trial hypocenters of neighbouring events (solid circles). Linking with cross-correlation data is shown with solid lines and linking with catalog data is shown with dashed lines. The ray paths from the events to station  $k$  and  $l$  are also shown, with  $dt$  being the travel-time difference between the events  $i$  and  $j$ . The slowness vectors from the initial location of the events corresponding to the ray path towards the stations are shown with thin arrows ( $s$ ). The thick arrows ( $\Delta \mathbf{x}$ ) are the relocation vectors, that represent the change in the  $x$ -direction to fit the data.

All double-difference equations (Equation (9)) for all event pairs per station are combined with the other stations. This forms a system of linear equations given by

$$\mathbf{W}\mathbf{G}\mathbf{m} = \mathbf{W}\mathbf{d}. \tag{10}$$

In this equation  $\mathbf{W}$  is a diagonal weighting matrix that weights every equation. Matrix  $\mathbf{G}$  contains all the partial derivatives and has a size of  $M \times 4N$ , where  $M$  is the number of double-difference observations and  $N$  is the number of events (with four hypocenter parameters per event).  $\mathbf{m}$  is the model vector with the changes in hypocenter parameters that have to be determined and  $\mathbf{d}$  is the data vector that contains the double-differences. Equation (10) is extended by  $4N$  additional equations (one for each origin time and coordinate direction) in order to constrain the mean shift of the earthquake locations during relocation to zero

$$\sum_{i=1}^N \Delta \mathbf{m}_i = 0. \quad (11)$$

Equation (11) is in most cases down-weighted during inversion, because in this way the cluster centroid is able to move slightly if the errors in the initial absolute locations of the clusters are significant.

In order to achieve a numerically stable solution there are a few steps that are done in the algorithm and also need to be considered when using it. First, the  $\mathbf{G}$  matrix is being scaled by normalization. This is done by applying a L2-norm to every column of  $\mathbf{G}$ . The L2-norm is a regularization method in which the square root of the sum of the squared column values is calculated. This is done because each equation only links two events together and thus there are only 8 elements per row of the  $4N$  columns in  $\mathbf{G}$  that have nonzero values, which makes the matrix highly sparse. When there is one earthquake event that is poorly linked to other events,  $\mathbf{G}$  becomes ill-conditioned. Depending on the solution method, the solution can become numerically unstable. The way to avoid this kind of ill-conditioned system is by only including events that are well linked to other events. This can be done by using events that have a minimum number of observations, which depends on the geometrical distribution of the stations that observe two linked events. Another method to regularize an ill-conditioned system is by damping the solution. Adding damping to Equation (10) gives the following equation

$$\mathbf{W} \begin{bmatrix} \mathbf{G} \\ \gamma \mathbf{I} \end{bmatrix} \mathbf{m} = \mathbf{W} \begin{bmatrix} \mathbf{d} \\ \mathbf{0} \end{bmatrix}, \quad (12)$$

where the damping factor is given by  $\gamma$  (the paper by [Waldhauser and Ellsworth \(2000\)](#) uses  $\lambda$  for the damping factor) and  $\mathbf{I}$  is the identity matrix. Damping the solution is typically necessary when the system is large.

If the clusters of events are small and the system is well-conditioned, Equation (10) can be solved by using the singular value decomposition (SVD) method

$$\hat{\mathbf{m}} = \mathbf{V} \mathbf{\Lambda}^{-1} \mathbf{U}^T \mathbf{d}. \quad (13)$$

In this equation,  $\mathbf{V}$  is a matrix filled with the orthogonal and normalized (orthonormal)

singular eigenvectors of  $\mathbf{G}^T\mathbf{G}$  and  $\mathbf{U}$  is a matrix containing the orthonormal singular eigenvectors of  $\mathbf{G}\mathbf{G}^T$ . The non-zero eigenvalues ( $\lambda_m^2$ ) of  $\mathbf{G}^T\mathbf{G}$  and  $\mathbf{G}\mathbf{G}^T$  are the same and the singular values ( $\lambda_m$ ) are stored in the diagonal matrix  $\Lambda$ . The least squares error for each model parameter  $i$  is calculated by

$$e_i^2 = C_{ii} \cdot var, \quad (14)$$

where the diagonal elements of the covariance matrix  $\mathbf{C} = \mathbf{V}\Lambda^{-2}\mathbf{V}^T$  are stored in  $C_{ii}$  and  $var$  is the variance of the weighted residuals. The covariance is used to determine the correlation between the variables and the variance is used to determine the spread of the data set.  $Var$  is calculated by

$$var = \frac{\sum_{i=1}^M (d_i - \bar{d})^2 - \frac{(\sum_{i=1}^M d_i - \bar{d})^2}{M}}{M - (4N)} \quad (15)$$

where  $\bar{d}$  is the mean of the residual vector and  $d_i$  is the residual belonging to the  $i$ th observation.

When the system becomes larger, it becomes computationally intractable to perform an SVD. In this case a solution is found by using the conjugate gradient method (LSQR) by [Paige and Saunders \(1982\)](#). A solution for  $\hat{m}$  is found by solving the damped least-squares problem, where the difference between the predicted and observed data is being minimized:

$$\left\| \mathbf{W} \begin{bmatrix} \mathbf{G} \\ \gamma \mathbf{I} \end{bmatrix} \mathbf{m} - \mathbf{W} \begin{bmatrix} \mathbf{d} \\ \mathbf{0} \end{bmatrix} \right\|_2 = 0. \quad (16)$$

### 2.1.2 HypoDD relocation procedure

There are four codes in the *hypoDD* algorithm created by [Waldhauser and Ellsworth \(2000\)](#): *hista2ddsta*, *ncsn2pha*, *ph2dt* and *hypoDD*. *Hista2ddsta* can convert standard hypoinverse station files to a station file format used by the programs *ph2dt* and *hypoDD* and *ncsn2pha* converts NCSN catalog data (from the Northern California Earthquake Catalog) to a file format that can be used by the programs *ph2dt* and *hypoDD*. The programs that are used in this research are *ph2dt* and *hypoDD* and will be explained further in this section.

The program *ph2dt* produces travel time differences between pairs of earthquakes from P- and S- phase picks and/or from waveform cross correlation data. The catalog data used in this research are put in a data file (*phase.dat*) that contains information about the origin time, location and errors of the events, as well as the P- wave phase picks per station and the weighting of these picks. The weighting of the individual picks is done by choosing a value between 0 and 1, where 0 means a phase pick with very poor quality (and larger uncertainty) and where 1 means a very good phase pick (and a small uncertainty). Location information about the stations are stored in a file called *station.dat*. *ph2dt* makes use of these two input

files to produce the travel time differences. The file *ph2dt.inp* is a control file containing the chosen parameters for the program *ph2dt*. There are seven parameters to set for this program, namely: **MINWGHT**, **MAXDIST**, **MAXSEP**, **MAXNGH**, **MINLNK**, **MINOBS** and **MAXOBS** (see Table 1 for the description of the parameters). The following points are important to consider when picking the right values for the parameters. To get strong linked event pairs it is important to keep the distance between the events as small as possible (**MAXSEP**) for which the minimum amount of links per event (**MINLNK**) can be established. Typically a strong link is defined by eight or more observations, i.e. one observation for each degree of freedom. However many observations for one event pair does not guarantee a stable solution, since the distribution of the stations is also one of the factors determining the stability of a solution. For large systems a maximum number of neighbors (**MAXNGH**) is usually set to eight, but when the system is small it is set equal to the amount of events and **MAXOBS** is set equal to the amount of stations.

**Table 1:** *Ph2dt* input parameters description for the *ph2dt.inp* input file.

<i>ph2dt</i> input parameters	
Parameter	Description
<b>MINWGHT</b>	Minimum pick weight
<b>MAXDIST</b>	Maximum distance (in km) between the event pairs and the stations
<b>MAXSEP</b>	Maximum hypocentral separation distance (in km) between event pairs
<b>MAXNGH</b>	Maximum number of neighbors per event
<b>MINLNK</b>	Minimum number of links required to define a neighbor
<b>MINOBS</b>	Minimum number of links per pair saved
<b>MAXOBS</b>	Maximum number of links per pair saved

The output files created by *ph2dt* are: a file with the travel times from selected event pairs (*dt.ct*), a summary of all events with their initial hypocenter locations (*event.dat*), a file with events that have at least the minimum amount of observations chosen (*event.sel*) and a log file that contains additional information like for example a list of outliers and amount of pairs (*ph2dt.log*). The outliers listed in *ph2dt.log* are removed by *ph2dt* and are identified as delay times that are larger than the minimum expected delay time for a certain event pair. The maximum expected delay time is calculated for a P- and S-wave that travel from the initial location with a P-wave velocity of 4 km/s and a S-wave velocity of 2.3 km/s, plus a 0.5 second cutoff to account for uncertainties in the initial hypocenter locations. These output files from *ph2dt* are used as input files for the program *hypoDD*.

The program *hypoDD* determines the double-difference hypocenter locations from the differential travel time data produced by *ph2dt*. The program minimizes the residuals between the observed and calculated travel time differences in an iterative way. It makes use of a 1-D velocity model that is defined in the control file.

The input files for *hypoDD* are *dt.ct*, *dt.cc*, *event.dat* and *station.dat*. The file *dt.cc* contains the travel time difference residual data from cross-correlations. The parameter settings for *hypoDD* are stored in the control file *hypoDD.inp*. An overview of the parameters is given in Table 2.

**Table 2:** *HypoDD* input parameters description for the *hypoDD.inp* input file.

<i>hypoDD</i> input parameters	
Parameter	Description
<b>IDAT</b>	Data type: 1 = cross correlation data; 2 = catalog data; 3 = both data types
<b>IPHA</b>	Phase type: 1 = P-wave; 2 = S-wave; 3 = both
<b>DIST</b>	Maximum distance between event cluster centroid and stations
<b>OBSCC, OBSCT</b>	Minimum number of cross-correlation and catalog observations per pair to form a cluster
<b>ISTART</b>	Initial locations: 1 = start from cluster centroid; 2 = start from catalog locations
<b>ISOLV</b>	Least squares solution method: 1 = SVD; 2 = LSQR
<b>NSET</b>	Number of sets of iterations
<b>NITER</b>	Number of iterations per set
<b>WTCCP, WTCCS</b>	Weight for cross-correlation data (P- and S-wave) during iteration
<b>WTCTP, WTCTS</b>	Weight for catalog data (P- and S-wave) during iteration
<b>WRCC, WRCT</b>	Cutoff threshold for outliers located on the tails of cross-correlation, catalog data
<b>WDCC, WDCT</b>	Maximum separation distance (in km) for cross-correlation, catalog data
<b>DAMP</b>	damping factor (only when LSQR method is used)
<b>NLAY</b>	Number of velocity model layers
<b>RATIO</b>	$V_P/V_S$ ratio, constant for all layers
<b>TOP</b>	Depth of the top of the layers (in km)
<b>VEL</b>	Layer P- wave velocities (km/s)
<b>CID</b>	Index of cluster to be relocated
<b>ID</b>	ID of events to be relocated

Next are a few important notes listed to consider when choosing the right parameters. Ill-conditioned systems are prevented by *hypoDD* by grouping events into clusters. The events within a cluster are linked to each other. The strength of the chain of links within a cluster is determined by a minimum amount of observations per event pair (**OBSCC**, **OBSCT**). Typical, the value of this minimum amount of observations is chosen to be equal to the number of degrees of freedom per event pair, which is three for spatial and one for time per event. Increasing the value could increase the stability of the solution, but it might split up the clusters into smaller sub-clusters. Decreasing the value might lead to including more events in a cluster, but it also decreases the stability of the solution. When the value of **OBSCT** is chosen to be larger than the value of **MAXOBS** (in *ph2dt.inp*) no clusters will be found by *hypoDD*. The best way is to give **OBSCT** a value that is equal or less than the value for **MINLNK** (in *ph2dt.inp*) to make sure that there are enough strong links between closeby events.

The connectivity between events also depends on the maximum hypocentral separation distance allowed between events that are linked. When this distance is small, then few events will be connected. The parameters **WDCT** and **WDCC** control the separation distance in *hypoDD*. Distances between events that are larger than the values of these parameters get removed by *hypoDD* during the first iteration. The parameter **WDCT** is the same as the parameter **MAXSEPT** in *ph2dt*. It is advised to give **MAXSEP** a larger value and experiment with smaller values for **WDCT**. Doing it this way will keep the separations distances small and still connect all events within **MAXSEP**. When LSQR is chosen as least squares solution method, then **DAMP** is the damping factor. Typically a damping factor between 1 and 100 is taken, but the exact value is problem-dependent. When a large damping factor is chosen, the hypocenter is restricted in deviation from the initial location.

The choice of the damping factor also depends on the condition of the system, which is expressed by the condition number (CND, which is an output of *hypoDD* and can be found in *hypodd.log*). The condition number is the ratio between the largest and smallest eigenvalue and is used to measure the sensitivity of the system to changes or errors in the data. Based on experiments, a CND between 40 and 80 is desirable and can be achieved by adjusting the damping factor.

The *a priori* weighting parameters are **WTCCP**, **WTCCS**, **WTCTP**, **WTCTS** and the re-weighting parameters are **WRCC**, **WRCT**, **WDCC**, **WDCT**. Typically for the first iteration set only the *a priori* weights are used, then the re-weighting parameters are used in the next sets of iterations.

Next is a description of the files that are created by *hypoDD*. Initial hypocenter locations are stored in the file *hypoDD.loc* and the relocated hypocenter locations are stored in the file *hypoDD.reloc*. Station residuals are stored in the file *hypoDD.sta* and data residuals are stored in *hypoDD.res*. The file *hypoDD.src* stores takeoff angle and azimuth information for each relocated event and the file *hypoDD.log* stores the run time information. The run time output gives information about the inversion in each iteration. Per iteration it gives information about the percentage of events used (also for catalog data and cross-correlation), the RMS residuals for the two data types, the largest RMS residual observed at a station, the absolute change of the event parameters, the absolute shift of the cluster origin, the number of earthquakes and the condition number. It is preferred that the percentage of events used doesn't decrease too much, that the RMS residuals for each data type decrease per iteration and that the changes in the event parameters are in the same order of the uncertainties of the initial locations for the first iterations. Damping the solution vector modifies how many iterations until a solution converges. Most of the shifts in hypocenter locations are within the first few iterations. Furthermore, the absolute shifts in the cluster origin should be small and thereby the least possible number of airquakes is preferred. Airquakes are event locations that relocate above the surface. This can happen when the velocity model is insufficient, when the damping value is too small, the seismic network is too sparse or has a low azimuthal coverage. Another possibility is that event pair, located near the surface, become airquakes, because the control in the vertical offset between the events is poor. There are a few solutions to prevent airquakes: increasing the damping factor, including more stations close to the event pairs or lowering the velocity of the first layer.

## 2.2 Data

The seismic data used to relocate the aftershocks are P-wave first arrivals from earthquakes with a magnitude  $\geq 2.5$ . From the hand-picked arrival times, travel times are determined using the origin times. The estimated initial locations and origin times from the aftershocks are from the [USGS Earthquake Catalog \(2017\)](#) and [ISC On-line Bulletin \(2016\)](#). There are three different datasets used in this research; one larger dataset (A) and two smaller datasets (B and C). The smaller datasets are used to find the right parameters settings for dataset A. Table A gives dataset A, the origin locations and times of the large dataset that contains all the earthquakes with a magnitude  $\geq 2.5$ . The estimated origin locations and times are determined with a fixed depth  $> 0.0$  km. The two smaller datasets are given in Table B and C (Appendix B and C). Table B gives the estimated initial locations and origin

times of the events with a fixed depth  $> 0.0$  km for events that have a magnitude  $\geq 3.0$  (dataset B). There are few aftershocks that have their estimated initial location and time being determined with a fixed depth at 0.0 km (dataset C). Since using these locations and times can produce different relocation results, a third dataset has been used that is listed in Table C.

A modified version of the 1-D P-wave velocity model determined for this region by Fadel (2018) is used for the relocation (Table G, Appendix G). Because *hypoDD* can only use velocity models up to 12 layers, the model by Fadel (2018) has been adjusted to this restriction and limited to a maximum depth of 60 km.

## 2.3 Stations

All stations that are within  $11^\circ$  distance from the Moiyabana earthquake are used in this research (Appendix D and E: Table D and Figure E), because within this epicentral distance the arrival times can be determined with a small uncertainty. The LBTB and NARS Botswana network stations are used to gain hand-picked arrival times. Arrival times from the remaining stations are from the ISC On-line Bulletin (2016).

The hand-picked arrival times from the LBTB and NARS Botswana stations are weighted according to the scheme in Table 3. The arrival times from the ISC On-line Bulletin (2016) are given a weight of 0.8, since the quality of every individual pick is unknown. An exception to this are the arrival times with a "impulsive" quality, which are given a weight of 1.

Because the distance between the main event and the stations is larger than 80 kilometers, there is a large event-to-station offset, and therefore the depths of the aftershocks cannot be determined accurately.

**Table 3:** Weight scheme for the hand-picked arrival times

Weight value	Uncertainty (sec)
0.1	$\geq 0.200$
0.5	0.050 - 0.200
1	$\leq 0.050$

### 3 Results

I determined appropriate relocation inversion parameters by using the smaller datasets B and C. The results of these tests are shown in Appendix F, G and H. Appendix F contains the results for dataset B which is solved with the LSQR method and Appendix G contains the results for dataset C which is solved with the SVD method. These two tests are done with data from the LBTB and NARS Botswana stations. Appendix H contains the results for dataset C, solved with the LSQR method and with data from all stations within 11° epicentral distance from the main event.

The results that are obtained by LSQR or SVD for datasets B and C are similar when the LBTB and NARS Botswana stations are used (Appendix F and Appendix G). The results where all the stations within 11° epicentral distance are used (Appendix H), show a more dispersed pattern of relocated hypocenters. Therefore, only data from the LBTB and NARS Botswana seismic stations were used for dataset A. Furthermore, the LSQR method was preferred because this method has the highest amount of relocated events (79.4%). From the 21.6 % that has not been relocated, is 1 event marked as an airquake and the remaining initial locations are too far away to be relocated.

The *ph2dt* and *hypoDD* parameters are similar for the larger and smaller dataset, except for the **DAMP** parameter, which is 15 instead of 10. Table 4 gives an overview of the parameter settings for dataset A. The results of the relocation are listed in Table 5 and Figure 6 shows both the estimated hypocenter locations and the relocated hypocenter locations in map view (Figure 6A) and cross-section (Figure 6B). 73.75% of the 80 earthquakes in dataset A have been relocated, 12.5% had their initial location too far from the clusters to be relocated and 13.75% got removed by *hypoDD* because they were relocated above the surface.

According to Paige and Saunders (1982), the accuracy of the standard errors for each model parameter that has been estimated with the LSQR method is not guaranteed. This is caused by the diagonal elements of the covariance matrix being computed approximately and depending on a proper convergence during the iterations. The reliability of the calculated errors can be evaluated by using the SVD method and its least squares errors calculations.

**Table 4:** Parameter settings for *ph2dt* (left table) and *hypoDD* (right table) for dataset A using the LSQR method. Parameter values with a \* are only used in the second iteration set.

<i>ph2dt</i> parameter	Value	<i>hypoDD</i> parameter	Value
MINWGHT	0	DIST	700
MAXDIST	700	OBST	8
MAXSEP	18	ISTART	1
MAXNGH	81	NSET	2
MINLNK	8	NITER	5
MINOBS	1	WRCT	3*
MAXOBS	22	WDCT	17*
		DAMP	15*

**Table 5:** The locations and origin times of the relocated events with the LSQR method and parameter settings given in Table 4. Errors are given in meters.

ID	Date	Origin time (UTC)	Latitude (°) ± error (m)	Longitude (°) ± error (m)	Depth (km) ± error (m)
2017/04/03Mw6.5	2017-04-03	17:40:14.80	-22.720 ± 693.4	25.126 ± 888.4	18.367 ± 744.7
2017/04/03mb4.7	2017-04-03	18:11:24.06	-22.646 ± 448.3	24.985 ± 485.5	7.004 ± 580.6
2017/04/03ML2.6	2017-04-03	19:14:56.48	-22.644 ± 326.8	24.986 ± 456.2	7.374 ± 647.7
2017/04/03ML3.5	2017-04-03	20:09:48.00	-22.637 ± 489.0	24.980 ± 573.6	10.153 ± 618.9
2017/04/03ML2.9_2	2017-04-03	21:01:11.06	-22.634 ± 486.7	24.985 ± 577.1	8.523 ± 766.3
2017/04/03ML2.7	2017-04-03	22:19:37.38	-22.624 ± 787.0	25.013 ± 955.2	10.256 ± 1208.4
2017/04/03mb4.0	2017-04-03	23:16:21.04	-22.714 ± 509.8	25.134 ± 546.0	14.790 ± 739.3
2017/04/04ML2.7_1	2017-04-04	01:59:57.06	-22.639 ± 639.3	24.952 ± 703.0	3.443 ± 589.0
2017/04/04ML3.3_1	2017-04-04	04:19:20.82	-22.702 ± 547.0	25.078 ± 653.8	10.657 ± 743.5
2017/04/04ML2.9_1	2017-04-04	09:32:00.39	-22.695 ± 440.6	25.127 ± 619.8	11.156 ± 655.9
2017/04/04ML3.3_2	2017-04-04	09:39:45.03	-22.654 ± 527.8	24.970 ± 661.3	1.618 ± 884.7
2017/04/04ML2.9_2	2017-04-04	13:56:27.61	-22.690 ± 635.6	25.123 ± 750.6	12.774 ± 879.8
2017/04/04ML3.1	2017-04-04	15:46:31.82	-22.711 ± 477.0	25.148 ± 482.0	10.874 ± 739.8
2017/04/04ML2.9_2	2017-04-04	18:07:22.52	-22.653 ± 554.0	25.012 ± 598.9	5.250 ± 643.9
2017/04/04ML3.5	2017-04-04	18:53:08.16	-22.662 ± 696.7	24.960 ± 764.1	4.815 ± 975.5
2017/04/04ML3.4	2017-04-04	19:41:57.84	-22.727 ± 571.4	25.125 ± 628.3	16.770 ± 807.5
2017/04/04ML2.8	2017-04-04	21:18:37.60	-22.625 ± 566.0	24.943 ± 678.1	10.303 ± 671.4
2017/04/04ML2.6	2017-04-04	22:13:55.32	-22.732 ± 375.9	25.134 ± 581.2	14.414 ± 650.8
2017/04/04ML2.5	2017-04-04	23:45:33.90	-22.703 ± 508.8	25.076 ± 519.4	18.142 ± 662.0
2017/04/05mb5.0	2017-04-05	00:55:48.87	-22.630 ± 418.3	25.993 ± 478.8	9.505 ± 472.5
2017/04/05ML2.9	2017-04-05	02:49:02.67	-22.748 ± 620.1	25.129 ± 672.8	17.529 ± 786.5
2017/04/05ML3.1	2017-04-05	15:02:34.82	-22.662 ± 528.1	24.884 ± 600.7	2.252 ± 780.2
2017/04/05ML3.2	2017-04-05	22:46:59.48	-22.653 ± 448.9	24.955 ± 558.4	4.702 ± 641.6
2017/04/06ML3.1	2017-04-06	05:25:58.39	-22.713 ± 724.0	25.106 ± 854.3	15.520 ± 1034.8
2017/04/06ML3.9	2017-04-06	07:33:59.59	-22.681 ± 472.3	25.021 ± 548.5	12.961 ± 607.5
2017/04/06ML2.6	2017-04-06	11:47:48.03	-22.680 ± 643.0	25.133 ± 722.3	8.197 ± 757.1
2017/04/07ML3.5	2017-04-07	02:08:17.58	-22.643 ± 468.3	24.967 ± 577.0	10.280 ± 561.7
2017/04/07ML3.2	2017-04-07	21:08:48.88	-22.746 ± 617.4	25.060 ± 659.2	13.446 ± 825.7
2017/04/08ML2.6	2017-04-08	16:22:19.79	-22.643 ± 403.5	25.013 ± 551.3	10.073 ± 440.9
2017/04/08ML2.5	2017-04-08	16:50:26.37	-22.697 ± 495.1	25.150 ± 627.1	7.969 ± 1060.5
2017/04/08mb4.7	2017-04-08	19:55:30.12	-22.629 ± 485.2	24.995 ± 559.2	10.158 ± 373.9
2017/04/09ML2.5	2017-04-09	07:03:08.70	-22.694 ± 604.9	25.151 ± 731.2	7.904 ± 949.5
2017/04/10ML2.9	2017-04-10	02:59:09.23	-22.634 ± 330.8	24.987 ± 437.1	9.751 ± 578.1
2017/04/10ML3.0	2017-04-10	20:54:30.72	-22.654 ± 547.3	24.998 ± 606.8	5.846 ± 549.6
2017/04/13ML2.6	2017-04-13	18:41:19.12	-22.712 ± 606.9	25.098 ± 681.8	17.212 ± 686.1
2017/04/18ML2.5	2017-04-18	07:42:06.83	-22.643 ± 484.1	25.100 ± 551.0	9.937 ± 561.1
2017/04/24ML3.1	2017-04-24	09:04:21.05	-22.735 ± 365.7	25.128 ± 491.7	15.870 ± 611.2
2017/04/24ML2.8	2017-04-24	17:53:38.88	-22.737 ± 356.4	25.128 ± 474.8	16.411 ± 566.4
2017/04/27ML2.7	2017-04-27	05:34:33.12	-22.616 ± 1041.1	24.960 ± 1348.9	11.844 ± 1146.8
2017/05/01ML2.8	2017-05-01	02:30:35.83	-22.763 ± 519.4	25.077 ± 589.7	15.877 ± 689.0
2017/05/05ML2.6	2017-05-05	16:40:08.41	-22.738 ± 584.7	25.126 ± 583.8	15.415 ± 687.0

**Table 5:** continued

ID	Date	Origin time (UTC)	Latitude ( $^{\circ}$ ) $\pm$ error (m)	Longitude ( $^{\circ}$ ) $\pm$ error (m)	Depth (km) $\pm$ error (m)
2017/05/06ML3.2	2017-05-06	18:00:02.04	-22.631 $\pm$ 431.4	25.000 $\pm$ 490.3	6.478 $\pm$ 391.3
2017/05/07ML2.5	2017-05-07	14:52:36.19	-22.685 $\pm$ 372.7	25.047 $\pm$ 424.8	10.832 $\pm$ 553.4
2017/05/09ML2.5	2017-05-09	00:21:46.74	-22.668 $\pm$ 398.2	25.007 $\pm$ 473.7	8.267 $\pm$ 590.8
2017/05/18ML3.4	2017-05-18	23:20:48.06	-22.658 $\pm$ 629.7	25.012 $\pm$ 753.4	0.107 $\pm$ 611.1
2017/05/24ML2.8	2017-05-24	08:10:36.01	-22.740 $\pm$ 469.6	25.125 $\pm$ 518.0	17.774 $\pm$ 521.8
2017/06/21mb4.2	2017-06-21	07:10:29.57	-22.735 $\pm$ 505.5	25.125 $\pm$ 573.0	18.053 $\pm$ 710.2
2017/06/24ML3.0	2017-06-24	10:32:19.11	-22.639 $\pm$ 632.4	25.022 $\pm$ 671.6	10.745 $\pm$ 687.2
2017/06/29ML2.8	2017-06-29	00:22:02.04	-22.636 $\pm$ 412.4	25.048 $\pm$ 487.1	13.161 $\pm$ 427.9
2017/07/04mb4.9	2017-07-04	11:37:04.23	-22.631 $\pm$ 401.1	25.040 $\pm$ 495.9	14.217 $\pm$ 435.0
2017/07/14ML3.3	2017-07-14	19:52:44.06	-22.720 $\pm$ 386.7	25.121 $\pm$ 515.2	18.306 $\pm$ 565.3
2017/08/03ML3.7	2017-08-03	23:30:41.86	-22.655 $\pm$ 842.0	24.990 $\pm$ 1039.7	4.416 $\pm$ 666.9
2017/08/09ML2.6	2017-08-09	22:25:02.38	-22.637 $\pm$ 414.1	25.005 $\pm$ 502.9	12.863 $\pm$ 479.3
2017/08/12mb4.9	2017-08-12	02:37:46.81	-23.592 $\pm$ 3483.2	25.684 $\pm$ 3952.8	12.616 $\pm$ 4224.7
2017/08/12ML2.6	2017-08-12	02:46:31.20	-23.584 $\pm$ 4745.6	25.679 $\pm$ 3714.9	14.800 $\pm$ 5144.3
2017/10/26ML3.0	2017-10-26	06:33:59.89	-22.670 $\pm$ 1008.6	25.016 $\pm$ 1288.3	18.239 $\pm$ 1329.9
2017/11/01mb4.7	2017-11-01	12:12:39.77	-22.692 $\pm$ 340.6	25.033 $\pm$ 456.5	11.610 $\pm$ 521.4
2017/11/02ML2.9	2017-11-02	19:37:53.48	-22.687 $\pm$ 504.5	25.023 $\pm$ 588.8	10.920 $\pm$ 681.8
2017/11/09ML2.8	2017-11-09	08:29:53.64	-22.632 $\pm$ 792.4	25.054 $\pm$ 749.1	12.496 $\pm$ 810.6

Figure 6A shows the initial locations and the calculated locations in map view. It shows the location of the two separate geographical clusters. The smaller cluster is located 113 km away from the main event. It also shows that the previously more dispersed locations are now relocated closer together inside each cluster. The extent of the events in the larger cluster is 24 km and the events are aligned along a NW-SE strike. The aftershocks are located towards the northwest and decrease in depth in the northwest direction. From cross-section X–Y it can be seen that the hypocenters in the larger cluster are also relocated closer together. The previously more random located events, from which most had a fixed depth, are now relocated along a vertical line dipping towards to northeast. The depth range is from  $0.107 \pm 0.611$  km to  $18.367 \pm 0.744$  km and all the aftershocks are relocated at a shallower depth than the main event. A few smaller earthquakes are relocated outside the cluster’s main dipping alignment. Along with some more smaller earthquakes that are located close to the main event, these events appear to be relocated along a vertical dipping line towards the southwest. The depth extent of these events could approximately go from 8 km to 17 km.

### 3.1 Robustness

The robustness of the results can be determined in different ways. Changing the seismic station distribution, the velocity model, initial hypocenter locations and number of events are a few of them. The results that are calculated with different methods and settings show many similarities. For example, the alignment of the larger cluster along a NW-SE strike, the smaller aftershocks being located at shallower depths than the main event, the decrease of event depth towards the northwest of the larger cluster and the alignment of the event depths along a vertical line dipping towards the northeast. Since these similarities persist when different methods and settings are used, it can be said that the results are quite robust.

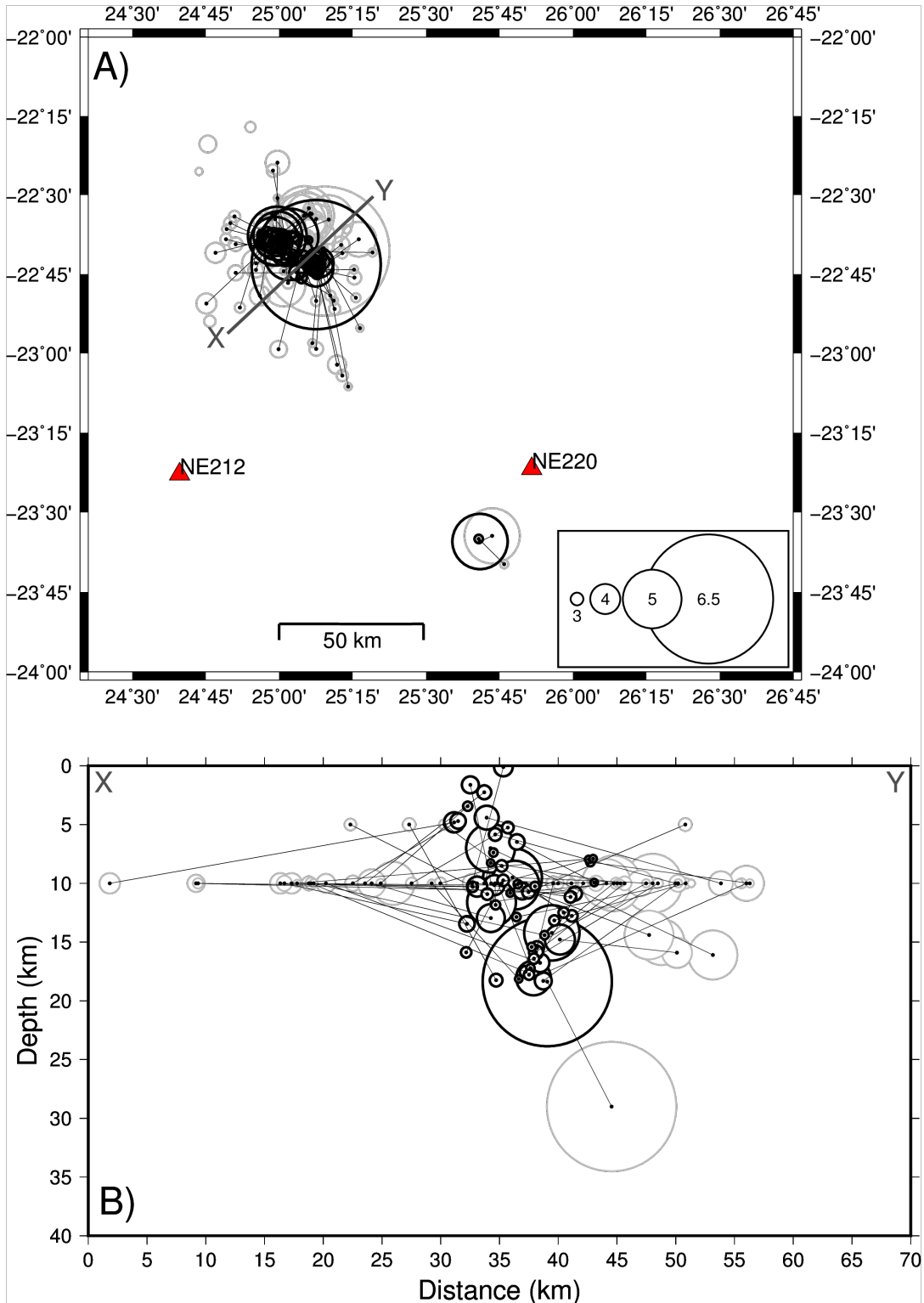


**Figure 6:** Estimated hypocenter locations of the large dataset linked to their relocated hypocenter locations. A) Map view of estimated epicenter locations (light grey circles) linked to their relocated epicenter locations (black circles). The red triangles represent the locations of nearby NARS Botswana seismic stations. B) Cross-section (X–Y) where the estimated hypocenters (light grey circles) are linked to their relocated hypocenter locations (black circles). The size of the circles represents the magnitudes of the events.

## 4 Discussion

The results in color, to display the depths of the relocated events and the focal mechanisms of events *2017/04/03Mw6.5* and *2017/08/12mb4.9* [H. Paulssen, personal communication] are visible in Figure 7. A detailed map of the large cluster is given in Figure 8A and the cross-section X–Y is given in Figure 8B. The strike, along which the hypocenters of the large cluster are located, is consistent with the focal mechanisms that are determined for the main event and several aftershocks (Figure 8A). The vertical dip at which the hypocenters are relocated, corresponds well with the focal mechanisms and the dip of the main event (Figure 8B). The small magnitude events that form a dipping structure towards the southwest could possibly have occurred on a antithetic fault.

As stated in the Methods section 2.3, the distance between the main event and the seismic station is large ( $\geq 80$  km), which limits the accuracy of the hypocenter depth that can be achieved. Also, the accuracy of the errors of the results that are calculated with the LSQR method is not guaranteed. The errors calculated with the SVD method are more reliable and give a better idea about the order of magnitude of the errors. However, the alignment of the hypocenters and the similarity of the results for various parameter settings gives credibility to the results.

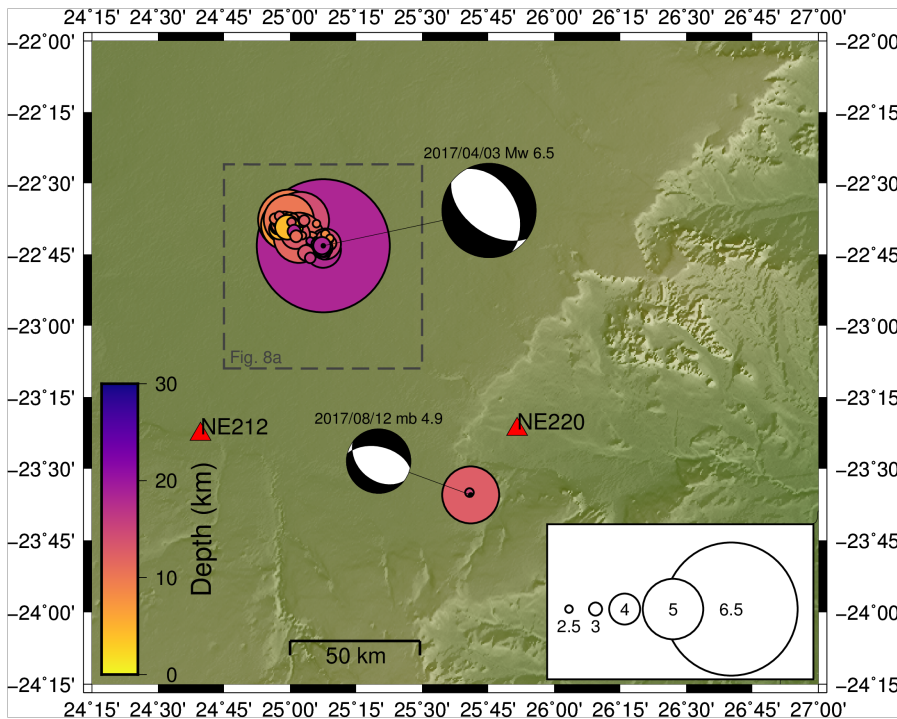


**Figure 7:** Map view of the relocated hypocenter locations for the 2017 Moyiabana earthquake and its aftershocks. Every colored circle represents an earthquake. The depth of each event is given by a color and the magnitude of each earthquake is given by the size of the circle. The focal mechanisms of the main event (*2017/04/03Mw6.5*) and event *2017/08/12mb4.9* are shown as the black and white beach balls.

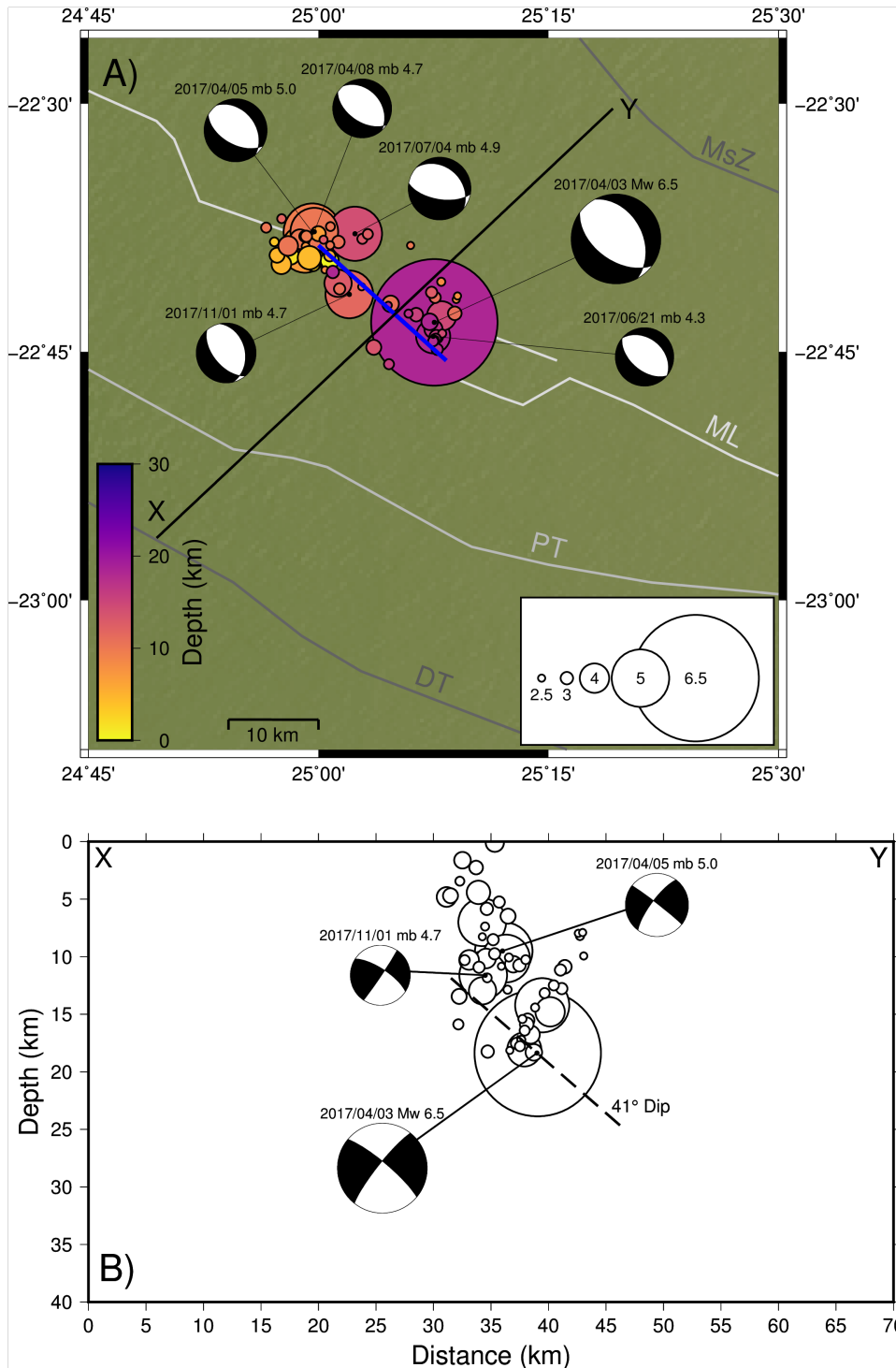


**Figure 8:** A) Relocated hypocenter locations for the 2017 Moiyabana earthquake and its aftershocks in the area of the grey dashed line box in Figure 7. Every earthquake is represented by a colored circle. The colors inside the circles give the depth of the hypocenter. The magnitude of every earthquake is indicated by the size of the circles. Grey lines represent the local fault structures interpreted by Kolawole et al. (2017). DT = Dinokwe Thrust; ML = Moiyabana Lineament; MsZ = Mahalapye Shear Zone; PT = Paleoproterozoic Thrust. The thick blue line is the fault trace of the Moiyabana Lineament that has been determined with InSAR measurements by Kolawole et al. (2017). B) Cross-section X–Y. The dip of the 2017 Moiyabana earthquake is shown as a dashed line. In both figures the (projected) focal mechanisms of the 2017 Moiyabana earthquake and a few aftershocks [H. Paulssen, personal communication] are displayed.

The geometry of the large cluster corresponds well with the interpreted Moiyabana Lineament by Kolawole et al. (2017). Cross-section X–Y is similar to the cross-section from the aeromagnetic data by Kolawole et al. (2017), so the results can directly be compared. Figure 9 shows the two results superimposed, highlighting that the relocated hypocenters of the large cluster are nearly consistent with the interpreted tectonic structure of the Moiyabana Lineament. From this comparison we interpret that the 2017 Moiyabana earthquake and its aftershocks occurred on the Moiyabana lineament which is a normal fault that dips towards the northeast.

According to the geological map that has been created by Ranganai et al. (2002) and Leseane et al. (2015), event *2017/08/12mb4.9* occurred inside the Kaapvaal Craton (Figure 2). The focal mechanism that has been determined for event *2017/08/12mb4.9* does not seem to correspond with the interpreted faults structures by Ranganai et al. (2002) (Figure 4). In Figure 4 event *2017/08/12mb4.9* is placed close to the interpreted shear zone, whereas the focal mechanism suggest that the event occurred on a normal fault that dips either to the southwest or northeast.

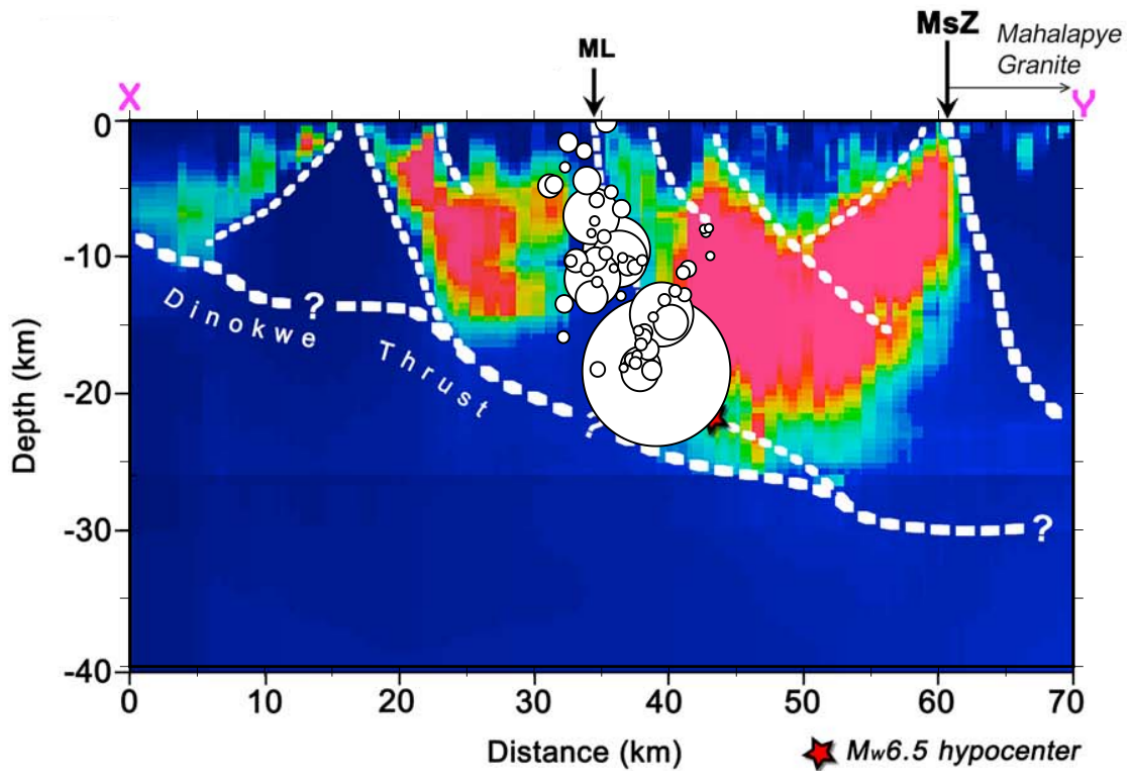


**Figure 9:** Cross-section X–Y with the results from this research on top of the aeromagnetic image from Kolawole et al. (2017) with interpreted tectonic terrain boundaries and associated structures (white dotted lines). The scale for the magnetic susceptibility (SI) is given in blue to red (0 - 0.003). ML = Moiyabana Lineament; MsZ = Mahalapye Shear Zone.

Whether the events in the second cluster belong to aftershock sequence of the 2017 Moiyabana earthquake depends on the ability of the lithosphere to transfer the stresses over a distance of more than 100 km. According to a Coulomb stress analysis done to the 2014  $M_w$  6.2 Chiang Rai, Thailand intra-plate earthquake, the extent of the stress change was  $\sim 40$  km [Pananont et al. (2017)]. It would be interesting to conduct a Coulomb stress analysis for the 2017 Moiyabana earthquake sequence to get more insight in the possibility of event *2017/08/12mb4.9* and *2017/08/12ML2.6* being triggered by the main event.

The 2017 Moiyabana earthquake had a total duration of  $\sim 10$  s and is characterized by two asperities [Materna et al. (2019)]. The first one occurred in the lower crust and second one occurred shallower, indicating that the rupture propagated up-dip. Furthermore, the observation in this study that the aftershocks are relocated at a shallower depth than the main event suggests that the ruptures along the Moiyabana Fault in general have an up-dip propagation, but not necessarily when you look at the order of time of the aftershock occurrence.

From magnetotelluric data, Moorkamp et al. (2019) inferred that the Proterozoic Limpopo-Shashe belt contains continental accretion structures associated with the collision of the Kaapvaal and Zimbabwe Cratons and that the 2017 Moiyabana normal fault earthquake would have reactivated an existing thrust fault. This interpretation has also been made by Kolawole et al. (2017). Moorkamp et al. (2019) also found low velocities, trending NW–SE, and relatively high resistivity in the upper-most mantle below the main event at 75 km depth, what is interpreted as reduced grain size indicating weaker material compared to the surrounding material. A low-velocity anomaly is also observed in the upper asthenosphere beneath the ORZ [Yu et al. (2017)], but then between 150 and 400 km depth, which is interpreted as decompression melting induced by lithospheric thinning that results from the relative motion between the Archean Congo and Kalahari Cratons. But since there is no sign of a significant deep lithospheric thermal anomaly below the 2017 Moiyabana earthquake, it has been suggested that the triggering is initiated from the top by interaction of the ambient stress field with the ancient structures and not by thermal weakening from below [Moorkamp et al. (2019)].

In the World Stress Map 2008 [Heidbach et al. (2010)] three over-coring measurements are shown from mines in Botswana that have their horizontal stresses well aligned with the stress field needed to cause the 2017 Moiyabana earthquake. Unfortunately, because of significant errors in over-coring measurements and difficulties in verifying the details of the measurement procedure, the stress measurements in Botswana have been down-graded [Materna et al. (2019)] and are removed from the World Stress Map 2016 [Heidbach et al. (2016)]. But deviatoric stress models of Africa, made by Stamps et al. (2014), do show a general east-west tension in Botswana, which matches well with the observed extensional fault movement. Further research on the stress state can give more insight in the stresses and associated deformation in Botswana.

Even though the 2017 Moiyabana earthquake is located more than 300 km away from the ORZ, it has also been suggested that stress field is imposed by the southward-propagation of the EARS [Bird et al. (2006); Materna et al. (2019)].

## 5 Conclusions

The aftershocks of the  $M_w$  6.5 2017 Moiyabana, Botswana earthquake, with magnitudes  $\geq 2.5$ , have been located with the double-difference earthquake relocation algorithm *hypoDD*. There are two separate geographical clusters of events. The larger cluster contains the main event plus 56 aftershocks and is situated in the Limpopo-Shashe belt, whereas the smaller cluster is located 113 km southeast from the main event in the Kaapvaal Craton and contains only two earthquakes. The extent of the events in the larger cluster is 24 km and the events occurred along a NW–SE normal fault, consistent with the focal mechanism of the main event. The aftershocks occurred northwest of the main event and they decrease in depth in northwest direction. The relocated hypocenters show that the events occurred on a northeast dipping fault. From these results I infer that the 2017 Moiyabana earthquake and its aftershocks occurred on the reactivated, northeast dipping Moiyabana Fault. This fault is part of a Proterozoic zone of weakness, that contains ancient thrust faults associated with the collision of the Kaapvaal and Zimbabwe Cratons and responded to large scale extensional forces that are present in southern Africa.

## References

- Bird, P., Ben-Avraham, Z., Schubert, G., Andreoli, M., and Viola, G. (2006). Patterns of stress and strain rate in southern Africa. *Journal of Geophysical Research: Solid Earth*, 111(B8).
- England, P. and Jackson, J. (2011). Uncharted seismic risk. *Nature Geoscience*, 4(6):348.
- Fadel, I. E. A. M. (2018). Crustal and upper mantle structure of Botswana: is Botswana rifting?
- Fréchet, J. (1985). *Sismogenese et doublets sismiques*. PhD thesis, Universite Scientifique et Medicale de Grenoble.
- Frémont, M.-J. and Malone, S. D. (1987). High precision relative locations of earthquakes at Mount St. Helens, Washington. *Journal of Geophysical Research: Solid Earth*, 92(B10):10223–10236.
- Gomberg, J. S., Shedlock, K. M., and Roecker, S. W. (1990). The effect of S-wave arrival times on the accuracy of hypocenter estimation. *Bulletin of the Seismological Society of America*, 80(6A):1605–1628.
- Got, J.-L., Fréchet, J., and Klein, F. W. (1994). Deep fault plane geometry inferred from multiplet relative relocation beneath the south flank of Kilauea. *Journal of Geophysical Research: Solid Earth*, 99(B8):15375–15386.
- Heidbach, O., Rajabi, M., Ziegler, M., and Reiter, K. (2016). The World Stress Map database release 2016-global crustal stress pattern vs. absolute plate motion. In *EGU General Assembly Conference Abstracts*, volume 18, page 4861.
- Heidbach, O., Tingay, M., Barth, A., Reinecker, J., Kurfeß, D., and Müller, B. (2010). Global crustal stress pattern based on the World Stress Map database release 2008. *Tectonophysics*, 482(1-4):3–15.
- ISC On-line Bulletin (2016). *International Seismological Centre*. <http://www.isc.ac.uk> (accessed September and November 2018).
- Kinabo, B. D., Atekwana, E. A., Hogan, J. P., Modisi, M. P., Wheaton, D. D., and Kampunzu, A. (2007). Early structural development of the Okavango rift zone, NW Botswana. *Journal of African Earth Sciences*, 48(2-3):125–136.
- Kolawole, F., Atekwana, E. A., Malloy, S., Stamps, D. S., Grandin, R., Abdelsalam, M. G., Leseane, K., and Shemang, E. M. (2017). Aeromagnetic, gravity, and Differential Interferometric Synthetic Aperture Radar analyses reveal the causative fault of the 3 April 2017 Mw 6.5 Moiyabana, Botswana, earthquake. *Geophysical Research Letters*, 44(17):8837–8846.

- Leseane, K., Atekwana, E. A., Mickus, K. L., Abdelsalam, M. G., Shemang, E. M., and Atekwana, E. A. (2015). Thermal perturbations beneath the incipient Okavango Rift Zone, northwest Botswana. *Journal of Geophysical Research: Solid Earth*, 120(2):1210–1228.
- Linol, B. et al. (2013). *Sedimentology and sequence stratigraphy of the Congo and Kalahari basins of south Central Africa and their evolution during the formation and break-up of west Gondwana*. PhD thesis, Faculty of Sciences at the Nelson Mandela Metropolitan University, Port Elisabeth, South Africa, pp. 375.
- Materna, K., Wei, S., Wang, X., Heng, L., Wang, T., Chen, W., Salman, R., and Bürgmann, R. (2019). Source characteristics of the 2017 Mw6.4 Moijabana, Botswana earthquake, a rare lower-crustal event within an ancient zone of weakness. *Earth and Planetary Science Letters*, 506:348–359.
- McCourt, S. and Vearncombe, J. R. (1992). Shear zones of the Limpopo Belt and adjacent granitoid-greenstone terranes: implications for late Archaean collision tectonics in southern Africa. *Precambrian Research*, 55(1-4):553–570.
- Moorkamp, M., Fishwick, S., Walker, R. J., and Jones, A. G. (2019). Geophysical evidence for crustal and mantle weak zones controlling intra-plate seismicity—the 2017 Botswana earthquake sequence. *Earth and Planetary Science Letters*, 506:175–183.
- Paige, C. C. and Saunders, M. A. (1982). LSQR: An algorithm for sparse linear equations and sparse least squares. *ACM Transactions on Mathematical Software (TOMS)*, 8(1):43–71.
- Pananont, P., Herman, M., Pornsopin, P., Furlong, K., Habangkaem, S., Waldhauser, F., Wongwai, W., Limpisawad, S., Warnitchai, P., Kosuwan, S., et al. (2017). Seismotectonics of the 2014 Chiang Rai, Thailand, earthquake sequence. *Journal of Geophysical Research: Solid Earth*, 122(8):6367–6388.
- Pavlis, G. L. (1986). Appraising earthquake hypocenter location errors: A complete, practical approach for single-event locations. *Bulletin of the Seismological Society of America*, 76(6):1699–1717.
- Poupinet, G., Ellsworth, W., and Frechet, J. (1984). Monitoring velocity variations in the crust using earthquake doublets: An application to the Calaveras Fault, California. *Journal of Geophysical Research: Solid Earth*, 89(B7):5719–5731.
- Ranganai, R. T., Kampunzu, A., Atekwana, E. A., Paya, B., King, J., Koosimile, D., and Stettler, E. H. (2002). Gravity evidence for a larger Limpopo Belt in southern Africa and geodynamic implications. *Geophysical Journal International*, 149(3):F9–F14.
- Roering, C., Van Reenen, D., Smit, C., Barton Jr, J., De Beer, J., De Wit, M., Stettler, E., Van Schalkwyk, J., Stevens, G., and Pretorius, S. (1992). Tectonic model for the evolution of the Limpopo Belt. *Precambrian Research*, 55(1-4):539–552.

- Stamps, D., Flesch, L., Calais, E., and Ghosh, A. (2014). Current kinematics and dynamics of Africa and the East African Rift System. *Journal of Geophysical Research: Solid Earth*, 119(6):5161–5186.
- USGS Earthquake Catalog (2017). *US Geological Survey earthquake catalog*. <https://earthquake.usgs.gov/earthquakes/> (accessed May 10, 2018).
- Waldhauser, F. (2001). hypoDD—A Program to Compute Double-Difference Hypocenter Locations (hypoDD version 1.0-03/2001). *US Geol. Surv. Open File Rep.*, 01, 113.
- Waldhauser, F. and Ellsworth, W. L. (2000). A double-difference earthquake location algorithm: Method and application to the northern Hayward fault, California. *Bulletin of the Seismological Society of America*, 90(6):1353–1368.
- Yu, Y., Liu, K. H., Huang, Z., Zhao, D., Reed, C. A., Moidaki, M., Lei, J., and Gao, S. S. (2017). Mantle structure beneath the incipient Okavango rift zone in southern Africa. *Geosphere*, 13(1):102.

# Appendix A

**Table A:** Event information of the  $M_w$  6.5 Moiyabana, Botswana earthquake and the 80 aftershocks with magnitude  $\geq 2.5$  (dataset A). The date, origin time, latitude, longitude, depth and magnitude information are from the [ISC On-line Bulletin \(2016\)](#) and [USGS Earthquake Catalog \(2017\)](#). All earthquakes that have been located with the LSQR method have a \* behind their ID name. The events from the [ISC On-line Bulletin \(2016\)](#) and [USGS Earthquake Catalog \(2017\)](#) with a fixed depth, are marked with a  $\diamond$ .

ID	Date	Origin time (UTC)	Latitude ( $^\circ$ )	Longitude ( $^\circ$ )	Depth (km)	M
2017/04/03Mw6.5*	2017-04-03	17:40:18.56	-22.678	25.156	29.0	6.5 Mw
2017/04/03mb5.0	2017-04-03	17:50:16.96	-22.142	25.147	10.0 $^\diamond$	5.0 mb
2017/04/03ML3.8	2017-04-03	17:57:52.40	-22.610	25.119	10.0 $^\diamond$	3.8 ML
2017/04/03mb4.7*	2017-04-03	18:11:26.14	-22.578	25.169	16.1	4.7 mb
2017/04/03ML3.6	2017-04-03	18:20:47.80	-23.176	25.059	10.0 $^\diamond$	3.6 ML
2017/04/03mb4.6	2017-04-03	18:38:12.26	-22.567	25.099	15.0	4.6 mb
2017/04/03ML2.6*	2017-04-03	19:14:54.30	-22.654	24.986	10.0 $^\diamond$	2.6 ML
2017/04/03ML2.9.1	2017-04-03	19:39:33.50	-22.553	25.033	10.0 $^\diamond$	2.9 ML
2017/04/03ML3.5*	2017-04-03	20:09:47.70	-22.683	24.783	10.0 $^\diamond$	3.5 ML
2017/04/03ML2.9.2*	2017-04-03	21:01:09.50	-22.568	24.848	10.0 $^\diamond$	2.9 ML
2017/04/03ML2.9.3	2017-04-03	21:20:59.30	-22.899	24.764	10.0 $^\diamond$	2.9 ML
2017/04/03ML2.7*	2017-04-03	22:19:41.80	-22.825	25.261	10.0 $^\diamond$	2.7 ML
2017/04/03mb4.0*	2017-04-03	23:16:22.84	-22.576	25.126	15.9	4.0 mb
2017/04/04ML2.7.1*	2017-04-04	01:59:55.70	-22.608	24.821	10.0 $^\diamond$	2.7 ML
2017/04/04ML3.3.1*	2017-04-04	04:19:22.70	-22.987	24.998	10.0 $^\diamond$	3.3 ML
2017/04/04ML2.7.2	2017-04-04	06:40:45.40	-23.179	24.732	10.0 $^\diamond$	2.7 ML
2017/04/04ML2.9.1*	2017-04-04	09:32:00.10	-22.860	25.189	10.0 $^\diamond$	2.9 ML
2017/04/04ML3.3.2*	2017-04-04	09:39:44.40	-22.661	25.001	10.0 $^\diamond$	3.3 ML
2017/04/04ML2.9.2*	2017-04-04	13:56:24.50	-22.657	25.028	10.0 $^\diamond$	2.9 ML
2017/04/04ML3.1*	2017-04-04	15:46:33.70	-22.986	25.126	10.0 $^\diamond$	3.1 ML
2017/04/04ML2.9.2*	2017-04-04	18:07:23.00	-22.778	25.030	10.0 $^\diamond$	2.9 ML
2017/04/04ML3.5*	2017-04-04	18:53:07.30	-22.843	24.752	10.0 $^\diamond$	3.5 ML
2017/04/04ML3.4*	2017-04-04	19:41:58.10	-23.036	25.197	10.0 $^\diamond$	3.4 ML
2017/04/04ML2.8*	2017-04-04	21:18:37.80	-22.856	24.866	10.0 $^\diamond$	2.8 ML
2017/04/04ML2.6*	2017-04-04	22:13:56.60	-22.968	25.113	10.0 $^\diamond$	2.6 ML
2017/04/04ML2.5*	2017-04-04	23:45:31.80	-22.741	25.015	10.0 $^\diamond$	2.5 ML
2017/04/05mb5.0*	2017-04-05	00:55:50.44	-22.565	25.087	10.0 $^\diamond$	5.0 mb
2017/04/05ML2.6	2017-04-05	02:06:47.00	-22.802	24.978	10.0 $^\diamond$	2.6 ML
2017/04/05ML2.9*	2017-04-05	02:49:04.90	-23.070	25.215	10.0 $^\diamond$	2.9 ML
2017/04/05ML3.3	2017-04-05	12:26:41.90	-22.339	24.757	10.0 $^\diamond$	3.3 ML
2017/04/05ML3.1*	2017-04-05	15:02:34.60	-22.656	24.852	10.0 $^\diamond$	3.1 ML
2017/04/05ML3.2*	2017-04-05	22:46:59.80	-22.737	24.921	10.0 $^\diamond$	3.2 ML
2017/04/06mb4.5	2017-04-06	02:30:22.18	-22.785	25.016	10.0 $^\diamond$	4.5 mb
2017/04/06ML2.8	2017-04-06	03:53:47.90	-22.285	24.902	10.0 $^\diamond$	2.8 ML
2017/04/06ML3.1*	2017-04-06	05:25:54.70	-22.577	24.986	10.0 $^\diamond$	3.1 ML
2017/04/06ML3.9*	2017-04-06	07:33:58.40	-22.716	24.921	10.0 $^\diamond$	3.9 ML
2017/04/06ML2.6*	2017-04-06	11:47:50.70	-22.682	25.318	10.0 $^\diamond$	2.6 ML
2017/04/07ML3.5*	2017-04-07	02:08:17.10	-22.818	24.934	10.0 $^\diamond$	3.5 ML
2017/04/07ML2.6	2017-04-07	14:47:11.70	-22.934	24.905	10.0 $^\diamond$	2.6 ML
2017/04/07ML3.2*	2017-04-07	21:08:47.80	-22.746	24.852	10.0 $^\diamond$	3.2 ML
2017/04/08ML2.6*	2017-04-08	16:22:22.60	-22.653	25.028	10.0 $^\diamond$	2.6 ML
2017/04/08ML2.5*	2017-04-08	16:50:26.10	-22.921	25.275	10.0 $^\diamond$	2.5 ML
2017/04/08ML3.1	2017-04-08	17:31:26.20	-22.747	24.468	10.0 $^\diamond$	3.1 ML
2017/04/08mb4.7*	2017-04-08	19:55:32.78	-22.566	25.084	14.4	4.7 mb
2017/04/09ML2.5*	2017-04-09	07:03:14.20	-23.105	25.235	10.0 $^\diamond$	2.5 ML
2017/04/09ML2.6	2017-04-09	14:34:39.90	-22.024	24.878	10.0 $^\diamond$	2.6 ML

Table A: continued

ID	Date	Origin time (UTC)	Latitude (°)	Longitude (°)	Depth (km)	M
2017/04/10ML3.1	2017-04-10	02:51:01.90	-22.583	24.936	10.0°	3.1 ML
2017/04/10ML2.9*	2017-04-10	02:59:09.90	-22.559	24.973	10.0°	2.9 ML
2017/04/10ML3.0*	2017-04-10	20:54:32.50	-22.558	25.106	10.0°	3.0 ML
2017/04/12ML2.6	2017-04-12	03:40:22.00	-22.609	25.231	10.0°	2.6 ML
2017/04/13ML2.6*	2017-04-13	18:41:21.60	-22.834	25.186	10.0°	2.6 ML
2017/04/18ML2.5*	2017-04-18	07:42:05.50	-22.679	25.059	10.0°	2.5 ML
2017/04/20ML2.5	2017-04-20	09:34:19.90	-22.682	25.043	10.0°	2.5 ML
2017/04/24ML3.1*	2017-04-24	09:04:22.20	-22.761	25.256	10.0°	3.1 ML
2017/04/24ML2.8*	2017-04-24	17:53:39.70	-22.684	25.215	10.0°	2.8 ML
2017/04/27ML2.7*	2017-04-27	05:34:30.00	-22.643	24.987	10.0°	2.7 ML
2017/05/01ML2.8*	2017-05-01	02:30:37.80	-22.818	25.174	10.0°	2.8 ML
2017/05/05ML2.6*	2017-05-05	16:40:10.90	-22.736	25.255	10.0°	2.6 ML
2017/05/06ML2.5	2017-05-06	14:38:03.00	-22.705	25.277	10.0°	2.5 ML
2017/05/06ML3.2*	2017-05-06	18:00:04.70	-22.635	25.094	10.0°	3.2 ML
2017/05/07ML2.5*	2017-05-07	14:52:37.40	-22.668	25.152	10.0°	2.5 ML
2017/05/09ML2.5*	2017-05-09	00:21:46.50	-22.510	24.994	10.0°	2.5 ML
2017/05/10ML2.5	2017-05-10	04:39:14.60	-22.503	24.862	10.0°	2.5 ML
2017/05/18ML3.4*	2017-05-18	23:20:51.70	-22.696	25.015	10.0°	3.4 ML
2017/05/24ML2.8*	2017-05-24	08:10:36.50	-22.735	25.182	10.0°	2.8 ML
2017/06/21mb4.2*	2017-06-21	07:10:30.95	-22.640	25.271	10.0°	4.2 mb
2017/06/24ML3.0*	2017-06-24	10:32:14.30	-22.423	24.979	5.0°	3.0 ML
2017/06/29ML2.8*	2017-06-29	00:22:02.10	-22.542	25.101	10.0°	2.8 ML
2017/07/04mb4.9*	2017-07-04	11:37:05.22	-22.586	25.064	10.0°	4.9 mb
2017/07/14ML3.3*	2017-07-14	19:52:44.00	-22.658	25.211	10.0°	3.3 ML
2017/07/20ML2.5	2017-07-20	23:15:49.40	-22.566	25.132	10.0°	2.5 ML
2017/08/03ML3.7*	2017-08-03	23:30:41.10	-22.398	24.994	10.0°	3.7 ML
2017/08/09ML2.6*	2017-08-09	22:25:03.80	-22.560	25.111	10.0°	2.6 ML
2017/08/12mb4.9*	2017-08-12	02:37:47.14	-23.574	25.725	10.0°	4.9 mb
2017/08/12ML2.6*	2017-08-12	02:46:32.50	-23.663	25.766	10.0°	2.6 ML
2017/10/26ML3.0*	2017-10-26	06:33:55.60	-22.589	24.834	5.0°	3.0 ML
2017/11/01mb4.7*	2017-11-01	12:12:41.40	-22.637	25.108	10.0°	4.7 mb
2017/11/02ML2.5	2017-11-02	14:21:13.30	-22.426	24.727	5.0°	2.5 ML
2017/11/02ML2.9*	2017-11-02	19:37:54.80	-22.640	24.819	5.0°	2.9 ML
2017/11/09ML2.8*	2017-11-09	08:29:56.30	-22.835	25.126	5.0°	2.8 ML

## Appendix B

**Table B:** Event information of the  $M_w$  6.5 Moiyabana, Botswana earthquake and the 34 aftershocks with magnitude  $\geq 3.0$  (dataset B). The date, origin time, latitude, longitude, depth and magnitude information are from the [ISC On-line Bulletin \(2016\)](#) and [USGS Earthquake Catalog \(2017\)](#). All earthquakes that have been located with the LSQR method have a \* behind their ID name. The events from the [ISC On-line Bulletin \(2016\)](#) and [USGS Earthquake Catalog \(2017\)](#) with a fixed depth, are marked with a  $\diamond$ .

ID	Date	Origin time (UTC)	Latitude ( $^\circ$ )	Longitude ( $^\circ$ )	Depth (km)	M
2017/04/03Mw6.5*	2017-04-03	17:40:18.56	-22.678	25.156	29.0	6.5 Mw
2017/04/03mb5.0	2017-04-03	17:50:16.96	-22.142	25.147	10.0 $^\circ$	5.0 mb
2017/04/03ML3.8*	2017-04-03	17:57:52.40	-22.610	25.119	10.0 $^\circ$	3.8 ML
2017/04/03mb4.7*	2017-04-03	18:11:26.14	-22.578	25.169	16.1	4.7 mb
2017/04/03ML3.6	2017-04-03	18:20:47.80	-23.176	25.059	10.0 $^\circ$	3.6 ML
2017/04/03mb4.6*	2017-04-03	18:38:12.26	-22.567	25.099	15.0	4.6 mb
2017/04/03ML3.5*	2017-04-03	20:09:47.70	-22.683	24.783	10.0 $^\circ$	3.5 ML
2017/04/03mb4.0*	2017-04-03	23:16:22.84	-22.576	25.126	15.9	4.0 mb
2017/04/04ML3.3.1*	2017-04-04	04:19:22.70	-22.987	24.998	10.0 $^\circ$	3.3 ML
2017/04/04ML3.3.2*	2017-04-04	09:39:44.40	-22.661	25.001	10.0 $^\circ$	3.3 ML
2017/04/04ML3.1*	2017-04-04	15:46:33.70	-22.986	25.126	10.0 $^\circ$	3.1 ML
2017/04/04ML3.5	2017-04-04	18:53:07.30	-22.843	24.752	10.0 $^\circ$	3.5 ML
2017/04/04ML3.4*	2017-04-04	19:41:58.10	-23.036	25.197	10.0 $^\circ$	3.4 ML
2017/04/05mb5.0*	2017-04-05	00:55:50.44	-22.565	25.087	10.0 $^\circ$	5.0 mb
2017/04/05ML2.9*	2017-04-05	02:49:04.90	-23.070	25.215	10.0 $^\circ$	2.9 ML
2017/04/05ML3.3	2017-04-05	12:26:41.90	-22.339	24.757	10.0 $^\circ$	3.3 ML
2017/04/05ML3.1*	2017-04-05	15:02:34.60	-22.656	24.852	10.0 $^\circ$	3.1 ML
2017/04/05ML3.2*	2017-04-05	22:46:59.80	-22.737	24.921	10.0 $^\circ$	3.2 ML
2017/04/06mb4.5	2017-04-06	02:30:22.18	-22.785	25.016	10.0 $^\circ$	4.5 mb
2017/04/06ML3.1	2017-04-06	05:25:54.70	-22.577	24.986	10.0 $^\circ$	3.1 ML
2017/04/06ML3.9*	2017-04-06	07:33:58.40	-22.716	24.921	10.0 $^\circ$	3.9 ML
2017/04/07ML3.5*	2017-04-07	02:08:17.10	-22.818	24.934	10.0 $^\circ$	3.5 ML
2017/04/07ML3.2*	2017-04-07	21:08:47.80	-22.746	24.852	10.0 $^\circ$	3.2 ML
2017/04/08ML3.1	2017-04-08	17:31:26.20	-22.747	24.468	10.0 $^\circ$	3.1 ML
2017/04/08mb4.7*	2017-04-08	19:55:32.78	-22.566	25.084	14.4	4.7 mb
2017/04/10ML3.1*	2017-04-10	02:51:01.90	-22.583	24.936	10.0 $^\circ$	3.1 ML
2017/04/10ML3.0*	2017-04-10	20:54:32.50	-22.558	25.106	10.0 $^\circ$	3.0 ML
2017/04/24ML3.1*	2017-04-24	09:04:22.20	-22.761	25.256	10.0 $^\circ$	3.1 ML
2017/05/06ML3.2*	2017-05-06	18:00:04.70	-22.635	25.094	10.0 $^\circ$	3.2 ML
2017/05/18ML3.4*	2017-05-18	23:20:51.70	-22.696	25.015	10.0 $^\circ$	3.4 ML
2017/06/21mb4.2*	2017-06-21	07:10:30.95	-22.640	25.271	10.0 $^\circ$	4.2 mb
2017/07/04mb4.9*	2017-07-04	11:37:05.22	-22.586	25.064	10.0 $^\circ$	4.9 mb
2017/08/12mb4.9	2017-08-12	02:37:47.14	-23.574	25.725	10.0 $^\circ$	4.9 mb
2017/11/01mb4.7*	2017-11-01	12:12:41.40	-22.637	25.108	10.0 $^\circ$	4.7 mb

# Appendix C

**Table C:** Event information of the  $M_w$  6.5 Moiyabana, Botswana earthquake and the 34 aftershocks with magnitude  $\geq 3.0$  (dataset C). The date, origin time, latitude, longitude, depth and magnitude information are from the [ISC On-line Bulletin \(2016\)](#) and [USGS Earthquake Catalog \(2017\)](#). All earthquakes that have been located with the SVD method have a \* behind their ID name. The events from the [ISC On-line Bulletin \(2016\)](#) and [USGS Earthquake Catalog \(2017\)](#) with a fixed depth, are marked with a  $\circ$ .

ID	Date	Origin time (UTC)	Latitude ( $^\circ$ )	Longitude ( $^\circ$ )	Depth (km)	M
2017/04/03Mw6.5*	2017-04-03	17:40:18.56	-22.678	25.156	29.0	6.5 Mw
2017/04/03mb5.0	2017-04-03	17:50:16.96	-22.142	25.147	10.0 $^\circ$	5.0 mb
2017/04/03ML3.8	2017-04-03	17:57:52.40	-22.610	25.119	10.0 $^\circ$	3.8 ML
2017/04/03mb4.7*	2017-04-03	18:11:26.14	-22.578	25.169	16.1	4.7 mb
2017/04/03ML3.6	2017-04-03	18:20:47.80	-23.176	25.059	10.0 $^\circ$	3.6 ML
2017/04/03mb4.6	2017-04-03	18:38:12.26	-22.567	25.099	15.0	4.6 mb
2017/04/03ML3.5*	2017-04-03	20:09:47.70	-22.683	24.783	10.0 $^\circ$	3.5 ML
2017/04/03mb4.0*	2017-04-03	23:16:22.84	-22.576	25.126	15.9	4.0 mb
2017/04/04ML3.3.1	2017-04-04	04:19:22.70	-22.987	24.998	10.0 $^\circ$	3.3 ML
2017/04/04ML3.3.2*	2017-04-04	09:39:44.40	-22.661	25.001	10.0 $^\circ$	3.3 ML
2017/04/04ML3.1	2017-04-04	15:46:33.70	-22.661	25.001	10.0 $^\circ$	3.1 ML
2017/04/04mb3.8	2017-04-04	18:53:08.46	-22.5367	24.9746	0.0 $^\circ$	3.8 mb
2017/04/04mb3.7*	2017-04-04	19:41:56.11	-22.6012	25.3337	0.0 $^\circ$	3.7 mb
2017/04/05mb5.0*	2017-04-05	00:55:50.44	-22.565	25.087	10.0 $^\circ$	5.0 mb
2017/04/05mb3.7*	2017-04-05	02:49:02.38	-22.6913	25.1021	0.0 $^\circ$	3.7 mb
2017/04/05ML3.3	2017-04-05	12:26:41.90	-22.339	24.757	10.0 $^\circ$	3.3 ML
2017/04/05ML3.1	2017-04-05	15:02:34.60	-22.656	24.852	10.0 $^\circ$	3.1 ML
2017/04/05ML3.2	2017-04-05	22:46:59.80	-22.737	24.921	10.0 $^\circ$	3.2 ML
2017/04/06mb4.5	2017-04-06	02:30:22.18	-22.785	25.016	10.0 $^\circ$	4.5 mb
2017/04/06ML3.1	2017-04-06	05:25:54.70	-22.577	24.986	10.0 $^\circ$	3.1 ML
2017/04/06ML3.9*	2017-04-06	07:33:58.40	-22.716	24.921	10.0 $^\circ$	3.9 ML
2017/04/07ML3.5*	2017-04-07	02:08:17.10	-22.818	24.934	10.0 $^\circ$	3.5 ML
2017/04/07ML3.2*	2017-04-07	21:08:47.80	-22.746	24.852	10.0 $^\circ$	3.2 ML
2017/04/08ML3.1	2017-04-08	17:31:26.20	-22.747	24.468	10.0 $^\circ$	3.1 ML
2017/04/08mb4.7*	2017-04-08	19:55:32.78	-22.566	25.084	14.4	4.7 mb
2017/04/10ML3.1	2017-04-10	02:51:01.90	-22.583	24.936	10.0 $^\circ$	3.1 ML
2017/04/10ML3.0*	2017-04-10	20:54:32.50	-22.558	25.106	10.0 $^\circ$	3.0 ML
2017/04/24ML3.1*	2017-04-24	09:04:22.20	-22.761	25.256	10.0 $^\circ$	3.1 ML
2017/05/06ML3.2*	2017-05-06	18:00:04.70	-22.635	25.094	10.0 $^\circ$	3.2 ML
2017/05/18ML3.4	2017-05-18	23:20:51.70	-22.696	25.015	10.0 $^\circ$	3.4 ML
2017/06/21mb4.2*	2017-06-21	07:10:30.95	-22.640	25.271	10.0 $^\circ$	4.2 mb
2017/07/04mb4.9*	2017-07-04	11:37:05.22	-22.586	25.064	10.0 $^\circ$	4.9 mb
2017/08/12mb4.9	2017-08-12	02:37:47.14	-23.574	25.725	10.0 $^\circ$	4.9 mb
2017/11/01mb4.7*	2017-11-01	12:12:41.40	-22.637	25.108	10.0 $^\circ$	4.7 mb

# Appendix D

**Table D:** All station coordinates used in this research

station ID	Latitude (°)	Longitude (°)	station ID	Latitude (°)	Longitude (°)
NE201	-24.51535	23.93279	BRAK	-31.78100	22.89400
NE202	-24.11352	21.78230	GRAF	-32.27900	24.48990
NE203	-22.99307	20.19555	FRAZ	-31.92900	21.40800
NE204	-18.53956	21.33822	KOMG	-29.79700	17.48369
NE205	-18.62089	23.50048	ROOI	-32.49480	23.55160
NE206	-17.80017	25.16189	GRAN	-32.30200	22.17100
NE207	-19.52957	21.17400	CVNA	-31.48220	19.76170
NE208	-21.94641	25.44691	SOE	-32.71170	25.56170
NE209	-21.40355	23.77177	SUR	-32.38000	20.81167
NE210	-21.36192	21.21571	MERW	-32.67300	21.52300
NE211	-22.85382	22.20679	GRHM	-33.27680	26.37660
NE212	-23.38039	24.66079	TETE	-16.14700	33.57700
NE213	-25.47553	22.85729	KEIM	-28.70400	20.96800
NE214	-19.38931	22.16246	CNG	-26.29170	32.18830
NE215	-18.78417	25.19601			
NE216	-20.19568	24.53719			
NE217	-21.09968	27.33424			
NE218	-20.56285	26.21785			
NE219	-22.56967	27.44682			
NE220	-23.36303	25.85961			
NE221	-25.81185	24.80085			
LBTB	-25.01450	25.59700			
LEPH	-23.85820	27.79730			
KSR	-25.85169	26.89719			
HRAO	-25.89020	27.68590			
SLR	-25.73500	28.28170			
WDLM	-26.42380	27.42220			
MUSN	-22.28780	29.86000			
SWZ	-27.18231	25.33169			
PRYS	-26.92530	27.35980			
CRLN	-25.99490	30.02270			
PILG	-24.93200	30.70900			
MATP	-20.42583	28.49944			
MOPA	-23.51730	31.39770			
BOSA	-28.61370	25.25600			
I47ZA	-28.62110	25.23520			
SNKL	-28.27530	27.77140			
MMAL	-26.04890	31.20420			
HAGI	-26.11580	31.18950			
NWCL	-27.73600	29.89200			
UPI	-28.36200	21.25272			
ARMS	-28.04000	19.74000			
PKA	-29.67000	22.75670			
AUGR	-28.59400	20.33800			
WIN	-22.56670	17.10000			
POGA	-27.34600	31.70700			
TSUM	-19.20220	17.58380			
I35NA	-19.19130	17.57680			
HVD	-30.60500	25.49670			
LSZ	-15.27664	28.18822			
KSTD	-30.61730	29.30860			
BFON	-31.79890	23.68880			

# Appendix E

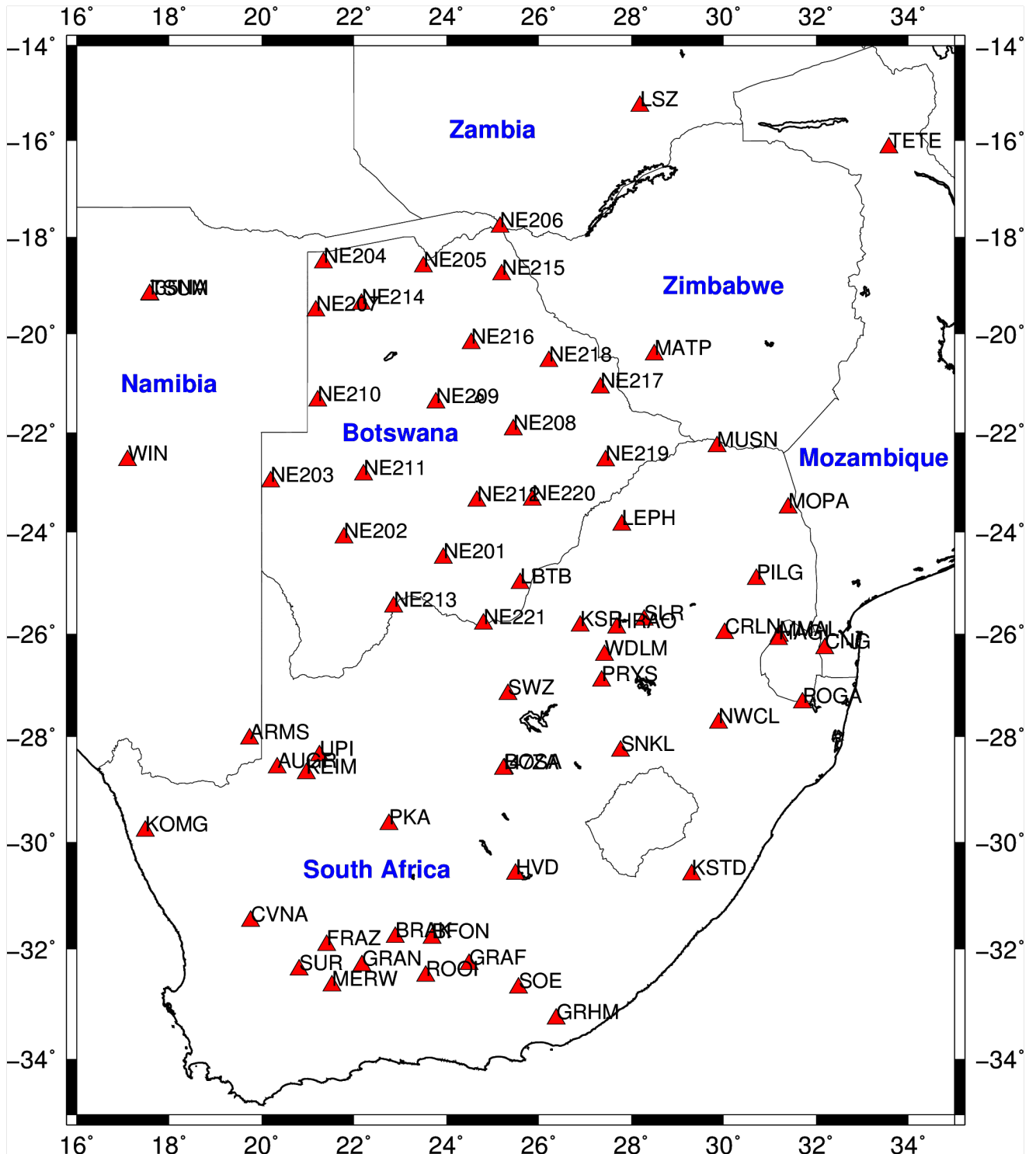


Figure E: Map with all stations locations used in this research.

## Appendix F

Results of the relocation solutions determined with the LSQR method for dataset B. The *ph2dt* and *hypoDD* parameter settings are given in Table F1. Results of the relocated events are listed in Table F2 and visualized in Figure F.

**Table F1:** Parameter settings for *ph2dt* (left table) and *hypoDD* (right table) for the LSQR method. Parameter values with a \* are only used in the second iteration set.

<i>ph2dt</i> parameter	Value	<i>hypoDD</i> parameter	Value
MINWGHT	0	DIST	700
MAXDIST	700	OBSCT	8
MAXSEP	18	ISTART	1
MAXNGH	34	NSET	2
MINLNK	8	NITER	5
MINOBS	1	WRCT	3*
MAXOBS	21	WDCT	17*
		DAMP	8*

**Table F2:** The locations and origin times determined with the LSQR method and parameter settings given in Table F1. Errors are given in meters.

ID	Date	Origin time (UTC)	Latitude (°) ± error (m)	Longitude (°) ± error (m)	Depth (km) ± error (m)
2017/04/03Mw6.5	2017-04-03	17:40:15.54	-22.716 ± 567.0	25.143 ± 595.9	24.425 ± 834.1
2017/04/03ML3.8	2017-04-03	17:57:53.12	-22.660 ± 720.3	25.029 ± 944.4	8.869 ± 948.7
2017/04/03mb4.7	2017-04-03	18:11:25.00	-22.638 ± 483.2	24.998 ± 522.1	14.037 ± 604.3
2017/04/03mb4.6	2017-04-03	18:38:09.86	-22.683 ± 950.4	24.996 ± 1017.1	0.630 ± 664.1
2017/04/03ML3.5	2017-04-03	20:09:48.74	-22.637 ± 727.6	25.005 ± 876.9	12.755 ± 919.7
2017/04/03mb4.0	2017-04-03	23:16:21.84	-22.709 ± 501.4	25.150 ± 493.5	21.347 ± 822.6
2017/04/04ML3.3_1	2017-04-04	04:19:22.10	-23.004 ± 3315.5	25.085 ± 3372.6	10.367 ± 4345.7
2017/04/04ML3.3_2	2017-04-04	09:39:46.35	-22.677 ± 693.7	25.043 ± 761.5	15.553 ± 761.8
2017/04/04ML3.1	2017-04-04	15:46:32.92	-23.017 ± 1694.6	25.152 ± 1993.3	8.570 ± 23.29.6
2017/04/04ML3.4	2017-04-04	19:41:58.48	-23.018 ± 3107.1	25.132 ± 2557.0	8.945 ± 3127.0
2017/04/05mb5.0	2017-04-05	00:55:49.72	-22.621 ± 607.0	25.006 ± 641.3	15.634 ± 577.2
2017/04/05ML2.9	2017-04-05	02:49:03.58	-23.034 ± 3041.9	25.134 ± 3356.9	13.474 ± 3650.0
2017/04/05ML3.1	2017-04-05	15:02:35.62	-22.676 ± 735.4	25.019 ± 798.7	4.195 ± 1195.8
2017/04/05ML3.2	2017-04-05	22:47:00.40	-22.656 ± 586.4	24.983 ± 728.7	8.532 ± 1057.4
2017/04/06ML3.9	2017-04-06	07:34:00.35	-22.681 ± 797.8	25.044 ± 854.9	16.562 ± 798.3
2017/04/07ML3.5	2017-04-07	02:08:18.34	-22.642 ± 691.2	24.988 ± 792.4	13.537 ± 857.4
2017/04/07ML3.2	2017-04-07	21:08:49.64	-22.746 ± 1012.0	25.083 ± 1093.6	17.148 ± 942.1
2017/04/08mb4.7	2017-04-08	19:55:30.96	-22.622 ± 515.2	25.010 ± 506.2	16.105 ± 518.7
2017/04/10ML3.1	2017-04-10	02:51:00.69	-22.657 ± 813.7	24.967 ± 887.3	1.497 ± 771.3
2017/04/10ML3.0	2017-04-10	20:54:31.82	-22.640 ± 575.2	25.012 ± 638.2	14.429 ± 595.5
2017/04/24ML3.1	2017-04-24	09:04:21.81	-22.731 ± 511.1	25.146 ± 478.1	21.975 ± 920.2
2017/05/06ML3.2	2017-05-06	18:00:03.00	-22.623 ± 538.1	25.012 ± 549.1	13.764 ± 608.2
2017/05/18ML3.4	2017-05-18	23:20:49.44	-22.656 ± 549.6	25.024 ± 629.9	8.642 ± 913.8
2017/06/21mb4.2	2017-06-21	07:10:30.30	-22.734 ± 442.7	25.147 ± 435.4	23.782 ± 854.5
2017/07/04mb4.9	2017-07-04	11:37:05.02	-22.625 ± 568.6	25.055 ± 590.9	20.260 ± 614.9
2017/11/01mb4.7	2017-11-01	12:12:40.58	-22.688 ± 563.0	25.048 ± 609.3	18.117 ± 723.9

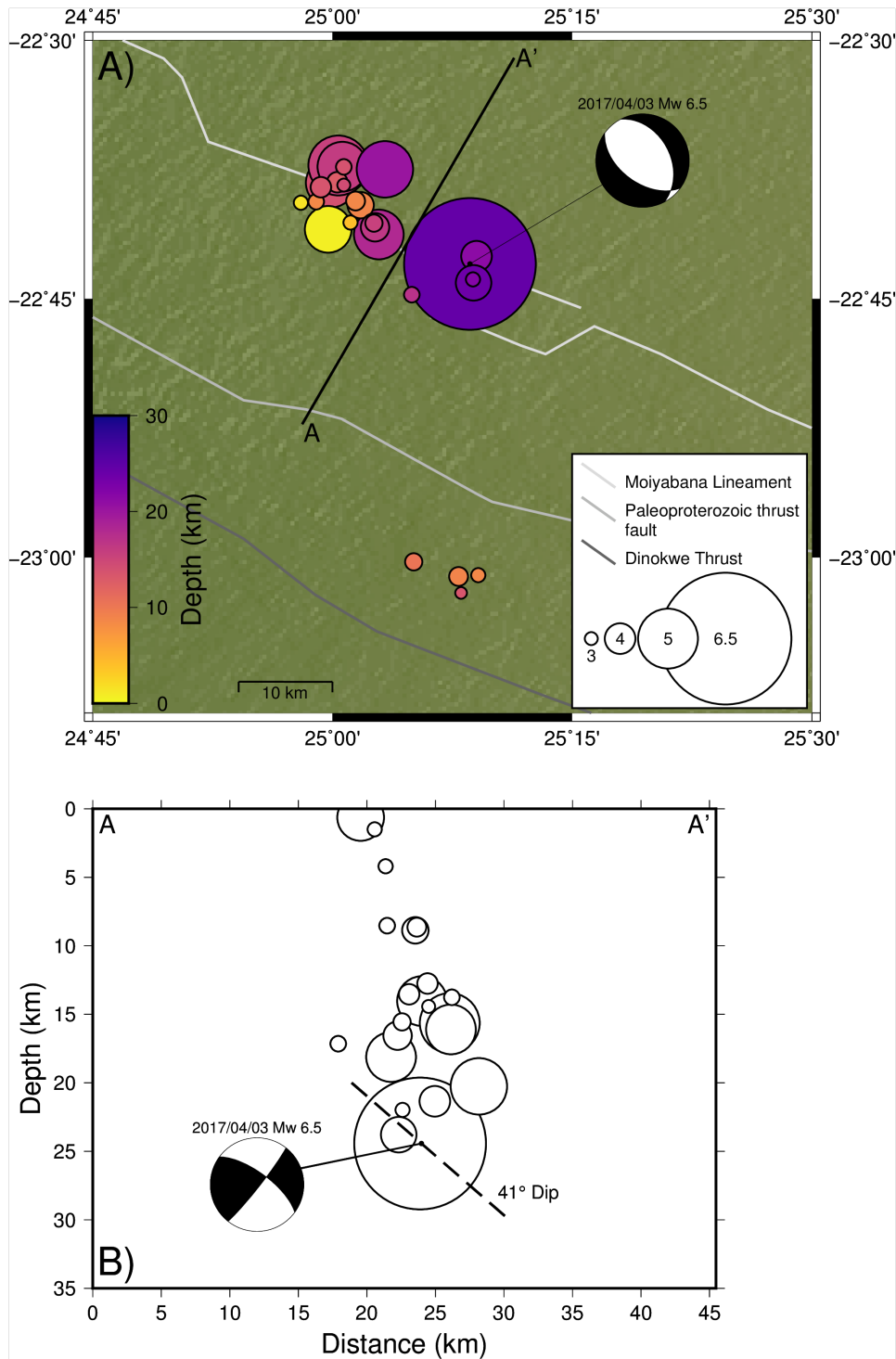


**Figure F:** A) Relocated hypocenter locations for the 2017 Moiyabana earthquake and its aftershocks which are listed in Table F2. Every earthquake is represented by a colored circle. The colors inside the circles give the depth of the epicenter. The magnitude of every earthquake is given by the size of the circles. Grey lines represent the local fault structures interpreted by Kolawole et al. (2017). B) Cross-section A-A'. The dip of the 2017 Moiyabana earthquake is given with a dashed line. In both figures the focal mechanism of the 2017 Moiyabana earthquake is displayed.

# Appendix G

Results of the solution determined with the SVD method for dataset C. *ph2dt* and *hypoDD* parameter settings are displayed in Table G1. Results of the relocated events are listed in Table G2 and visualized in Figure G.

**Table G1:** Parameter settings for *ph2dt* (left table) and *hypoDD* (right table). Parameter values with a \* are only used in the second iteration set.

<i>ph2dt</i> parameter	Value	<i>hypoDD</i> parameter	Value
MINWGHT	0	DIST	700
MAXDIST	700	OBSCT	8
MAXSEP	18	ISTART	2
MAXNGH	34	NSET	2
MINLNK	8	NITER	5
MINOBS	1	WRCT	3*
MAXOBS	21	WDCT	17*

**Table G2:** Relocated aftershock hypocenter and origin time solutions calculated with the SVD method for dataset C.

ID	Date	Origin time (UTC)	Latitude (°) ± error (m)	Longitude (°) ± error (m)	Depth (km) ± error (m)
2017/04/03Mw6.5	2017-04-03	17:40:15.16	-22.683 ± 137.2	25.129 ± 209.1	17.670 ± 268.9
2017/04/03mb4.7	2017-04-03	18:11:24.14	-22.604 ± 66.8	24.989 ± 78.2	3.204 ± 217.6
2017/04/03ML3.5	2017-04-03	20:09:48.36	-22.634 ± 183.9	25.058 ± 277.4	12.029 ± 324.4
2017/04/03mb4.0	2017-04-03	23:16:21.38	-22.676 ± 105.8	25.141 ± 118.6	14.216 ± 202.6
2017/04/04ML3.3_2	2017-04-04	09:39:45.81	-22.646 ± 61.2	25.039 ± 72.8	7.647 ± 128.5
2017/04/04ML3.7	2017-04-04	19:41:58.04	-22.670 ± 154.0	25.117 ± 148.2	15.563 ± 324.8
2017/04/05mb5.0	2017-04-05	00:55:49.06	-22.589 ± 64.0	24.998 ± 76.0	6.193 ± 164.2
2017/04/05ML3.7	2017-04-05	02:49:03.55	-22.714 ± 417.6	25.140 ± 408.7	16.359 ± 757.8
2017/04/06ML3.9	2017-04-06	07:33:59.90	-22.676 ± 103.1	25.094 ± 150.6	15.250 ± 212.9
2017/04/07ML3.5	2017-04-07	02:08:17.94	-22.640 ± 118.7	25.042 ± 168.5	12.366 ± 231.2
2017/04/07ML3.2	2017-04-07	21:08:49.12	-22.743 ± 159.5	25.136 ± 186.5	14.810 ± 371.4
2017/04/08mb4.7	2017-04-08	19:55:30.36	-22.589 ± 62.9	25.001 ± 74.8	7.270 ± 161.5
2017/04/10ML3.0	2017-04-10	20:54:31.04	-22.603 ± 65.3	24.999 ± 77.5	4.134 ± 210.6
2017/04/24ML3.1	2017-04-24	09:04:21.40	-22.700 ± 139.0	25.137 ± 150.6	15.608 ± 282.6
2017/05/06ML3.2	2017-05-06	18:00:02.00	-22.587 ± 73.7	25.002 ± 93.2	1.806 ± 283.6
2017/06/21mb4.2	2017-06-21	07:10:29.92	-22.703 ± 120.5	25.138 ± 129.3	17.748 ± 229.6
2017/07/04mb4.9	2017-07-04	11:37:04.56	-22.593 ± 67.9	25.047 ± 77.8	13.065 ± 98.3
2017/11/01mb4.7	2017-11-01	12:12:40.11	-22.655 ± 60.3	25.040 ± 70.6	10.532 ± 94.5

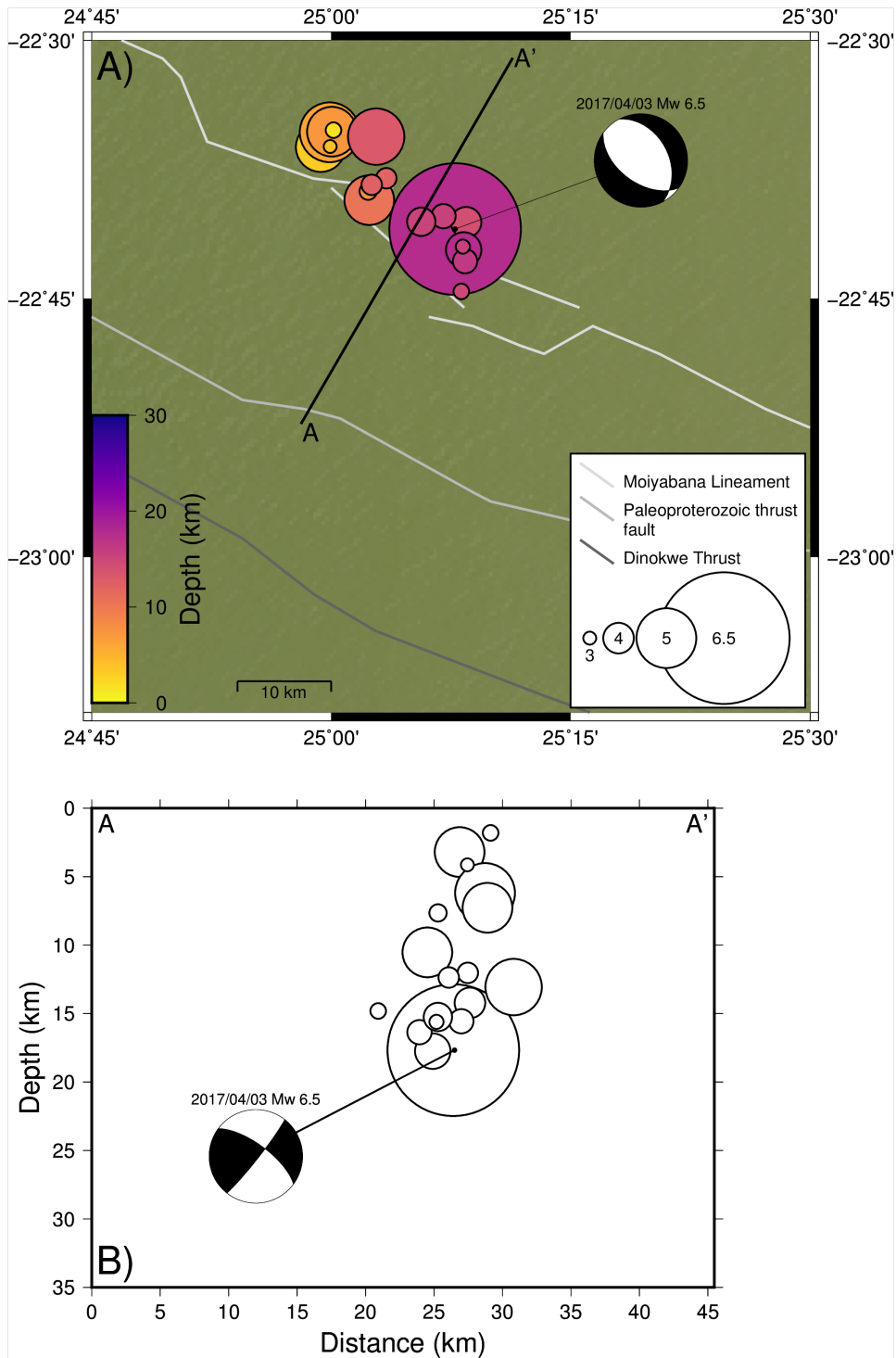


**Figure G:** Relocated hypocenter locations in map view and cross-section after using the SVD method for dataset C.

## Appendix H

Results of the solution determined with the LSQR method for dataset C, with data from all the stations listed in Table D. *ph2dt* and *hypoDD* parameter settings are displayed in Table H1. Results of the relocated events are listed in Table H2 and visualized in Figure H.

**Table H1:** Parameter settings for *ph2dt* (left table) and *hypoDD* (right table). Parameter values with a \* are only used in the second iteration set.

<i>ph2dt</i> parameter	Value	<i>hypoDD</i> parameter	Value
MINWGHT	0	DIST	1200
MAXDIST	1200	OBSCT	8
MAXSEP	18	ISTART	1
MAXNGH	34	NSET	2
MINLNK	8	NITER	5
MINOBS	1	WRCT	2*
MAXOBS	66	WDCT	17*
		DAMP	10*

**Table H2:** Relocated aftershock hypocenter and origin time solutions calculated with the LSQR method for dataset C with data from all the stations listed in Table D.

ID	Date	Origin time (UTC)	Latitude (°) ± error (m)	Longitude (°) ± error (m)	Depth (km) ± error (m)
2017/04/03Mw6.5	2017-04-03	17:40:15.56	-22.627 ± 5009.7	25.156 ± 3317.5	20.172 ± 3828.1
2017/04/03ML3.8	2017-04-03	17:57:52.82	-22.684 ± 2313.8	25.124 ± 2822.8	10.044 ± 4017.6
2017/04/03mb4.7	2017-04-03	18:11:24.76	-22.633 ± 1991.2	25.030 ± 2111.7	12.316 ± 2301.3
2017/04/03mb4.6	2017-04-03	18:38:10.20	-22.630 ± 2172.8	25.046 ± 2733.1	6.337 ± 2956.1
2017/04/03ML3.5	2017-04-03	20:09:48.30	-22.631 ± 2381.2	25.002 ± 2812.0	9.752 ± 3007.1
2017/04/03mb4.0	2017-04-03	23:16:21.60	-22.687 ± 2278.3	25.147 ± 2939.3	15.527 ± 3000.0
2017/04/04ML3.3_1	2017-04-04	04:19:22.02	-22.978 ± 1877.8	25.014 ± 2347.2	9.955 ± 2005.1
2017/04/04ML3.3_2	2017-04-04	09:39:46.08	-22.667 ± 1667.9	25.070 ± 1801.7	15.051 ± 2478.0
2017/04/04ML3.1	2017-04-04	15:46:32.98	-22.994 ± 1875.1	25.109 ± 2371.9	9.981 ± 2005.1
2017/04/04mb3.8	2017-04-04	18:53:09.32	-22.703 ± 2866.9	25.029 ± 2753.0	18.219 ± 3489.7
2017/04/05mb5.0	2017-04-05	00:55:49.47	-22.618 ± 2002.6	25.047 ± 2042.9	15.331 ± 2292.8
2017/04/05ML3.7	2017-04-05	02:49:03.56	-22.746 ± 3574.0	25.184 ± 4569.2	20.848 ± 4436.1
2017/04/05ML3.1	2017-04-05	15:02:35.39	-22.662 ± 2539.4	25.027 ± 2685.4	5.399 ± 4057.0
2017/04/05ML3.2	2017-04-05	22:47:00.08	-22.667 ± 1972.3	25.028 ± 2410.2	10.626 ± 2650.0
2017/04/06ML3.1	2017-04-06	05:25:58.59	-22.695 ± 3772.9	25.097 ± 4440.0	25.055 ± 4246.3
2017/04/06ML3.9	2017-04-06	07:33:59.94	-22.683 ± 2146.5	25.062 ± 2354.3	15.839 ± 2611.2
2017/04/07ML3.5	2017-04-07	02:08:17.95	-22.663 ± 2749.7	25.038 ± 2704.9	16.635 ± 2617.8
2017/04/07ML3.2	2017-04-07	21:08:49.24	-22.740 ± 2729.9	25.088 ± 3451.8	15.141 ± 2885.2
2017/04/08mb4.7	2017-04-08	19:55:30.68	-22.611 ± 1973.9	25.034 ± 2119.2	14.130 ± 2248.2
2017/04/10ML3.0	2017-04-10	20:54:31.56	-22.635 ± 1821.2	25.042 ± 1966.7	11.785 ± 2784.4
2017/04/24ML3.1	2017-04-24	09:04:21.42	-22.698 ± 3556.6	25.122 ± 4768.7	24.978 ± 3646.8
2017/05/06ML3.2	2017-05-06	18:00:02.48	-22.605 ± 2337.4	25.012 ± 2584.1	5.625 ± 4349.9
2017/06/21mb4.2	2017-06-21	07:10:30.10	-22.709 ± 2904.8	25.136 ± 3157.7	18.264 ± 3069.5
2017/07/04mb4.9	2017-07-04	11:37:04.76	-22.615 ± 1811.3	25.078 ± 2258.4	18.624 ± 2341.1
2017/11/01mb4.7	2017-11-01	12:12:40.32	-22.679 ± 1867.8	25.076 ± 1813.5	15.965 ± 2943.8

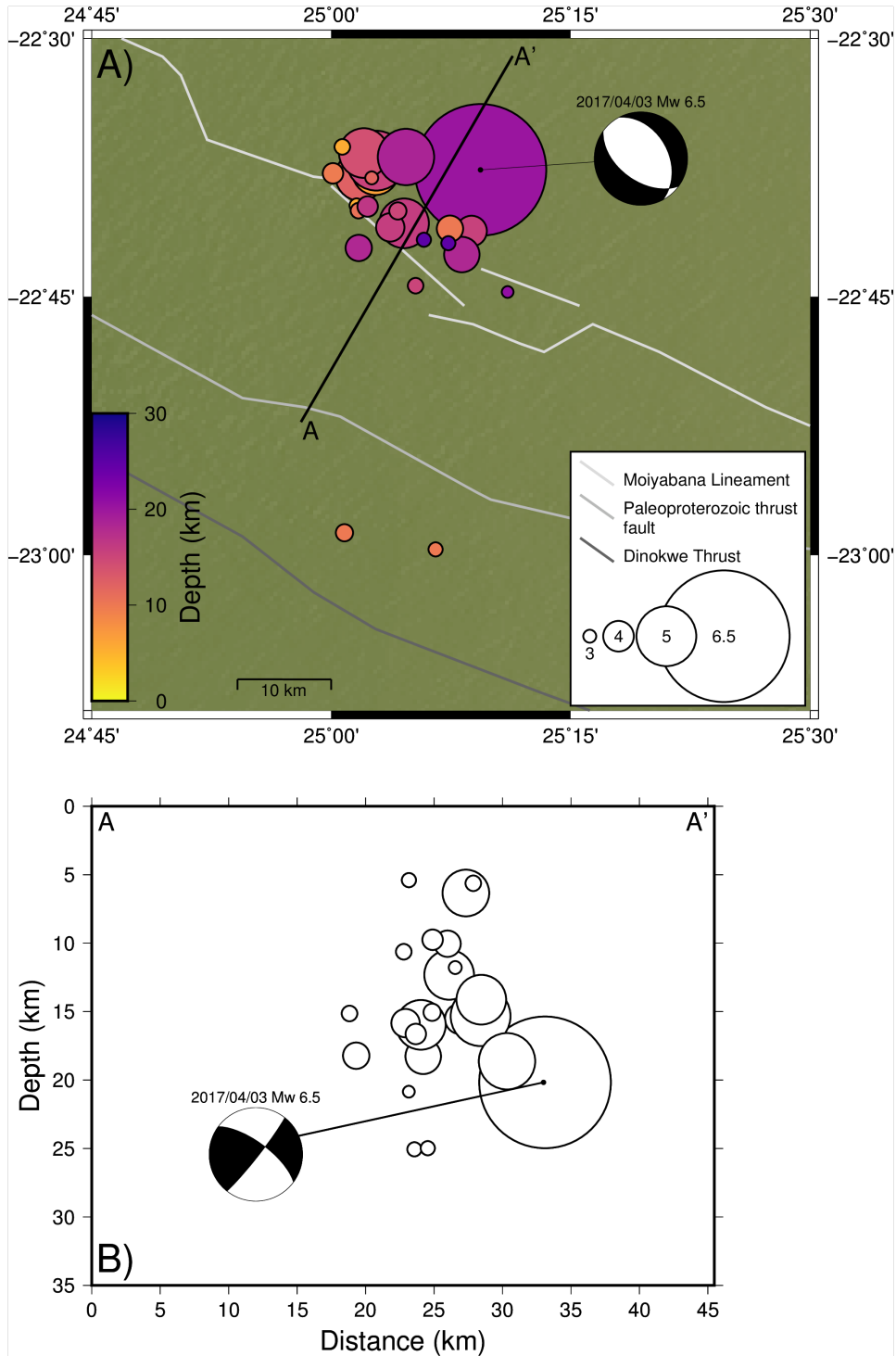


**Figure H:** Relocated hypocenter locations in map view and cross-section after using the LSQR method for dataset C with data from all the stations listed in Table D.

## Appendix G

**Table G:** The simplified 1-D local P-wave velocity model determined by [Fadel \(2018\)](#) that has been used for the relocation.

Depth top of layer (km)	P-wave velocity (km/s)
0.0	5.1513737471
1.0	5.3791153991
3.0	5.7375070690
5.0	6.1239498066
7.5	6.3320169211
10.0	6.4395163513
15.0	6.5055130034
25.0	6.6913793526
30.0	6.9716143192
35.0	7.3286593991
45.0	7.85
55.0	8.20